Revista Mexicana de Astronomía y Astrofísica, 62, 11-27, (2026)

OPEN ACCESS https://doi.org/10.22201/ia.30618649p.2026.62.01.02

Hadronic Clues in Quasars Caught by Fermi-LAT

A. Galván[1], N. Fraija[2], E. Aguilar-Ruiz[3], H. León Vargas[1], M. G. Dainotti[4,5] and J. A. de Diego[2]

[1] *Instituto de Física. Universidad Nacional Autónoma de México, Circuito de la Investigación Científica C. U., CdMx 04510, México.*
[2] *Instituto de Astronomía. Universidad Nacional Autónoma de México, Circuito de la Investigación Científica C. U., CdMx 04510, México.*
[3] *Instituto de Radioastronomía y Astrofísica. Universidad Nacional Autónoma de México, Antigua Carretera a Pátzcuaro 8701, Ex-Hda. San José de la Huerta, 58089, Morelia, Michoacán, México.*
[4] *Division of Science, National Astronomical Observatory of Japan, 2-21-1 Osawa, Mitaka, Tokyo 181-8588, Japan.*
[5] *The Graduate University for Advanced Studies (SOKENDAI), 2-21-1 Osawa, Mitaka, Tokyo 181-8588, Japan.*

Keywords: *High Energy Phenomena, Active Galactic Nuclei, Particle Acceleration : Non Thermal, Neutrinos, Gamma-rays.*

Abstract

This study explores whether hadronic processes could be responsible for the high-energy emission observed in quasars identified by the Large Area Telescope (LAT) instrument aboard the Fermi satellite. In contrast to purely leptonic models, this study investigates whether hadronic mechanisms can explain the observed gamma-ray spectra by analyzing the spectral energy distributions (SEDs) of a chosen sample of Flat-Spectrum Radio Quasars (FSRQs). By incorporating both hadronic and leptonic components into their multiwavelength modeling, we evaluated the model's feasibility to simultaneously describe the data collected by Fermi-LAT and neutrinos detected by IceCube. According to the results, a hadronic contribution is required to explain the SED of quasars detected by Fermi-LAT. However, their contribution to the neutrino flux detected by the IceCube remains underestimated.

Resumen

Este trabajo explora si los procesos hadrónicos podrían ser responsables de la emisión de alta energía observada en los cuásares identificados por el instrumento Large Area Telescope (LAT) a bordo del Satélite Fermi. En contraste con los modelos puramente leptónicos, el trabajo investiga si los mecanismos hadrónicos pueden explicar los espectros de rayos gamma observados, analizando las distribuciones espectrales de energía (SEDs) de una muestra escogida de FSRQs (Flat Spectrum Radio Quasars). Al incorporar componentes hadrónicos y leptónicos en su modelización multi-longitud de onda, evaluamos la viabilidad del modelo para describir simultáneamente los datos recogidos por Fermi-LAT y los neutrinos detectados por IceCube. Según los resultados, sería necesaria una contribución hadrónica para explicar la SED de los cuásares detectados por Fermi-LAT. Sin embargo, su contribución al flujo de neutrinos detectado por IceCube sigue siendo subestimada.

Corresponding author: Antonio Galván *E-mail address:* edwin@fisica.unam.mx
Received: April 16th, 2024 **Accepted:** February 20, 2026

1. Introduction

Victor Hess discovered high-energy Cosmic Rays (HECRs) over a century ago, but their origin is still a mystery. The interaction between cosmic rays (CRs) and magnetic fields makes it impossible to determine the location of CR production (Gaisser et al. 2013). Interactions between γ-ray photons and Cosmic Microwave Background (CMB) photons can reduce the intensity of γ-rays by a factor that depends both on the redshift and the energy of γ-rays (e.g. Gilmore et al. 2012; Franceschini & Rodighiero 2017). Since neutrinos have no net electric charge, they pass through magnetic fields unimpeded from their point of origin to Earth. Owing to their weak force and gravitational interactions with matter, neutrinos are not attenuated as they travel across the universe. The presence of high-energy neutrinos would provide hints for the search for astronomical UHCR accelerators (Halzen & Hooper 2002; Fraija et al. 2018).

To date, only one steady neutrino source has been identified, the Active Nuclei Galaxy (AGN) Seyfert type 2 NGC 1068, which is consistent with a neutrino cluster with a significance of 4.2 σ (IceCube Collaboration et al. 2022). Furthermore, on September 22, 2017, IceCube detected the neutrino IceCube-170922A with an energy above 0.1 PeV. The blazar TXS 0506 + 056 was in a flare state when the neutrino was detected, and its location was within the uncertainty of the neutrino arrival position. The probability of this conjunction is $\sim 3\sigma$ (IceCube Collaboration et al. 2018a). IceCube analyzed 9.5 years of data for TXS 0506+056 and detected an excess of neutrinos compared to the expected background (covering the period from September 2014 to March 2015). This variable flux indicates a 3.5σ neutrino emission from this blazar (IceCube Collaboration et al. 2018b) without an increase in its electromagnetic counterpart.

IceCube does not observe neutrinos directly but detects the Cherenkov light produced by secondary particles resulting from neutrino-nucleon interactions using its 5160 digital optical

modules (DOMs; IceCube Collaboration 2013). Neutrinos produce charged-current (CC) interactions with nuclei. The nucleus breaks apart, resulting in the release of a cascade of hadrons, with approximately 80% of the energy being transferred to the generated charged lepton For the case of ν_μ (as well as $\bar{\nu}_\mu$), secondary muons are created along the hadronic shower; these muons can travel several kilometers before decaying. Consequently, the detected light exhibited a track-like signature. In contrast, an electron (positron) neutrino ν_e ($\bar{\nu}_e$) causes an immediate electromagnetic cascade. This cascade overlaps with the hadronic cascade generated at the vertex. In the detector, this topology exhibits an elliptical shape. With the light deposited in the DOMs, the arrival position and energy of the neutrinos can be reconstructed. In the case of CC-ν_μ, the long light paths allow for a better reconstruction of the neutrino position in the sky, with errors $\mathcal{O}(1)$deg but with a worse energy reconstruction, because only a fraction of the track events lies in the instrument field of view. On the other hand, for CC-ν_e a better energy reconstruction is archived, but a worse arrival resolution is obtained, with median angular errors at the position of $\mathcal{O}(10-15)$deg(IceCube Collaboration 2013). Neutral-current (NC) cascades occur when neutrinos transfer only a small amount of energy to the nucleus before exiting. Therefore, we can expect only cascade topologies for all three types of neutrinos, with production at the vertex point limited to shower events (Bose & Rakshit 2021).

The Fermi Large Area Telescope (LAT) is a pair-conversion telescope that detects γ rays between 20 MeV and 300 GeV (Atwood et al. 2009). The fourth Fermi-LAT γ-ray source catalog (4FGL) (Abdollahi et al. 2020) uses Pass 8 data, which improved the angular resolution above 3 GeV, increased the acceptance by $\sim$ 20%, and expanded the effective area to 2.5 m^2 sr (2–300 GeV). Galactic diffuse emission modeling was refined, and energy dispersion effects were included for more accurate reconstruction. The catalog is based on eight years of data from 50 MeV to 1 TeV, along with subsequent updates: 4FGL-DR2 (10 years; Ballet et al. 2020) and 4FGL-DR3 (12 years; Abdollahi et al. 2022). A dedicated AGN subset, 4LAC (Ajello et al. 2020), covers sources in the 50 MeV–1 TeV range. In this paper, we describe the observations in § 2, outline the procedure for finding correlations with spatial arguments in § 3, present the physical formulation for describing the spectra of the candidates in correlation with neutrinos in § 4, and discuss our findings in § 5.

2. Observations

2.1. IceCube Neutrinos

The considerable angular uncertainties present in cascade-like topologies led us to omit them from this study. We are looking to conciliate point-like sources detected by Fermi-LAT with neutrinos detected by IceCube. This study examined the IceCube catalog IceCat-1 (Abbasi et al. 2023). This catalog contains 275 high-energy neutrinos exhibiting a track-like topology, recorded within a time frame from 2011 to 2023 in its initial release. The data is publicly accessible and regularly updated[1].

2.2. Fermi-LAT γ-rays

This work is based on the Second Data Release of the Fourth LAT AGN Catalog (4LAC-DR2; Lott et al. 2020), which extends the 4LAC catalog (Ajello et al. 2020) to ten years of Fermi-LAT observations. The original 4LAC catalog comprises 2,863 AGNs detected in γ-rays, including 665 flat-spectrum radio quasars (FSRQs), 1067 BL Lacertae objects (BL Lacs), 1077 blazar candidates of uncertain type (BCUs), and 64 other AGNs, such as radio galaxies and narrow-line Seyfert 1s. The 4LAC-DR2 release added 285 new AGNs, consisting of 39 FSRQs, 59 BL Lacs, 185BCUs, and 2 radio galaxies. In this work, we focus on the FSRQ population from the high-latitude subset of 4LAC-DR2 to ensure reliable source associations and well-constrained γ-ray spectra.[2] The spectra for each source were obtained through binned likelihood analysis following the standard steps of the Fermi-LAT Collaboration (as described below).[3] The data and the spacecraft files were obtained from the Fermi-LAT Data Server with pass 8[4]. The data set was selected at the neutrino position in the energy range of 100 MeV to 1 TeV and a mask radius of 15°. Likelihood analysis was performed using `Fermi Science Tools` (Fermi Science Support Development Team 2019) in the conda-based Python interface with version `2.2.0` of Fermi-tools. A selection of the data set was applied at the neutrino position in the energy range from 100 MeV to 1 TeV and a search radius of 15°. From this, only source events were retained (`evclass` = 128), and the types of events from the front and back sections of the tracker were converted to events within all subclasses PSF and Energy subclasses (`evtype` = 3). We also take into account, according to the Fermi-LAT team[5], a maximum zenith angle of 90°recommended for point like sources and a filter `(DATA_QUAL>0)&&(LAT_CONFIG==1)` on the Good Time Intervals centered at the position of the neutrino arrival position. A Region Of Interest (ROI)-based zenith cut was not applied. The angle of inclination between the source and LAT normal determines the response functions of the LAT instrument. The count of a source should depend on the time spent at a given inclination angle during the observation period. The livetime of the LAT, which refers to the duration observed at a specific sky position and inclination angle, is determined solely by its orientation history (it is independent of the source model). The tool gtltcube executes these corrections and is subsequently integrated into the pipeline. Finally, we computed the exposure map using the response function `P8R3_SOURCE_V3` within 40 ° of the ROI, considering ten energy bins.

To conduct the likelihood analysis, the ROI was modeled in an XML file, which incorporates the spectral properties of the gamma-ray sources listed in the 4FGL catalog, while allowing for the sources located within 5° of the neutrino arrival position. We also looked for a possible new gamma-ray source at the location of the neutrino arrival, and a new source was identified with a power-law spectral shape. The Galactic diffuse emission model used is `gll_iem_v07`, whereas the extragalactic isotropic diffuse emission model chosen is `iso_P8R3_SOURCE_V3_v1`. Taking this into account, the likelihood was calculated using the python interface `pyLikelihood`, which is part of the fermi-tools package (Fermi Science Support Development Team 2019). We iterated 50 times to determine that the likelihood converged. The first ten times we chose the `DRMNFB` minimizer, if this converges on these steps, we use the output as input for at least another interaction, but using `the NewMinuit` minimizer[6].

[1] https://dataverse.harvard.edu/dataset.xhtml?persistentId=doi:10.7910/DVN/SCRUCD

[2] The FITS tables for these catalogs are publicly available at https://fermi.gsfc.nasa.gov/ssc/data/access/lat/4LACDR2/.

[3] https://fermi.gsfc.nasa.gov/ssc/data/analysis/scitools/binned_likelihood_tutorial.html

[4] https://fermi.gsfc.nasa.gov/cgi-bin/ssc/LAT/LATDataQuery.cgi

[5] https://fermi.gsfc.nasa.gov/ssc/data/analysis/documentation/Cicerone/Cicerone_Data_Exploration/Data_preparation.html

[6] https://fermi.gsfc.nasa.gov/ssc/data/analysis/documentation/Cicerone/Cicerone_Likelihood/Fitting_Models.html

We built the light curves shown in Figures 2-19. Specifically, we analyzed the area surrounding the detected neutrino for 30 days before and after its arrival, focusing on the time reported by IceCube and using one-day intervals. We searched for emissions from a potential new gamma-ray source and examined the behavior of the 4FGL sources located within the error region of the reported position.

3. Analysis

To ascertain whether the FSRQ identified by Fermi-LAT serve as progenitors of neutrinos, we connected them to the IceCat-1 neutrino database provided by IceCube. In numerous instances, neutrinos and γ-ray sources do not converge. Nevertheless, the γ-ray sources are situated within the error region of the reconstructed neutrino position (e.g. IceCube Collaboration et al. 2018a; Garrappa et al. 2019; Sahakyan et al. 2023; Petropoulou et al. 2020). The methodology employed in this study to determine spatial coincidence is as follows.

Table 1 presents the correlation data along with the angular separation and localization of the neutrinos and 4FGL sources. The table displays neutrino events in the first column, followed by the (RA, Dec) best arrival direction reconstructed with a 90% confidence level uncertainty, and the best-fit energy reconstruction in the third column. The fourth column presents the 4FLG source associated with each neutrino, along with the celestial coordinates (RA, Dec) of the γ-ray source and the angular separation between the γ-ray source and neutrino arrival position. The counterpart and redshift of this source are presented. The counterpart is sourced from the 4LAC data, and the redshift is acquired from astronomical databases including NED[7] and CDS Portal[8], with queries performed using the 4FGL designation. With the exception of the γ-ray source 4FGL J1834.2+3136, the investigation was carried out using the name of the corresponding source.

To ensure thoroughness, we computed the likelihood of spatial correlation between a neutrino source and a gamma-ray source, employing the statistical methods adopted by Dichiara et al. (2020). To do this, we considered the neutrinos detected by IceCube listed in Table 1 together with the uncertainty in the reconstructed position of the neutrino. This motivated us to consider only events with track-type topologies, as these events have less uncertainty in locating the neutrino. After obtaining this population, we generated a synthetic distribution of gamma-ray sources that were uniformly spread throughout the celestial sphere, excluding galactic longitude values less than 10º, because we sought to recreate the FSRQs reported in the 4LAC (Ajello et al. 2022) on the objects with $|b| > 10$. Thus, a coincidence is considered if a synthetic gamma-ray source is located within the error region of the neutrino position. We repeated this action 1,000 times for each neutrino, calculating the probability as the ratio of favorable outcomes to total attempts throughout the process. The probability of serendipity is the value at which this ratio converges during the repetitions. Consequently, this probability is determined solely by the uncertainty associated with neutrinos. This implies that events with a high degree of uncertainty will be less significant, as there will be more sources of gamma rays within that portion of the solid angle.

The values in Table 2 were obtained by averaging each of the 1,000 steps, with the error indicating the standard deviation of these distributions. The convergence value of thousands of trials was visually determined, indicating that the number was sufficiently large for a clear trend to become evident. Cowan et al. (2011) considered rejection of the background hypothesis with a significance of at least 5σ as a suitable threshold to establish a discovery, which is equivalent to $p = 2.87 \times 10^{-7}$. To exclude a signal hypothesis, a threshold p-value of 0.05 (equivalent to a confidence level of 95%) is commonly used, corresponding to $1.64\,\sigma$.

Finally, we investigated evidence of a flaring condition in the gamma-ray source coinciding with IceCube's discovery of the neutrino. The temporal interval designated for the search for an electromagnetic equivalent in this study spans one week before and one week after the discovery of the neutrino by IceCube. For this investigation, we will utilize Fermi-LAT rate light curves within the energy range of 0.1 to 200 GeV of the LAT 4FGL-DR2 Catalog[9]. We investigated flares within a data-driven framework. This was done according to the baseline methodology. Meyer et al. (2019) presented the foundational technique and then compared it within the light curves derived in § 2.2 within the energy range of 100 MeV to 1 TeV. The authors used a continuous flux level criterion to determine the onset and end of the flare, depending on whether the flux exceeded or dropped below the threshold. This indicates that contiguous blocks constitute a peak if they exceed the baseline, and only those peaks that surpass this baseline are considered flares. In this study, we utilized the implementation created by (Wagner et al. 2022), who developed a code in Python[10] to identify flares utilizing Bayesian blocks and the Eisenstein-Hut HOP algorithm, which integrates a baseline state to detect flares exhibiting a rise and fall pattern superimposed on a quiescent state.

3.1. IC110807A

The event IC110807A was detected on 7 August 2011 at 21:36:00 UTC (MJD 55779.90), with an arrival direction RA, Dec = $(336.80^{\circ}{}^{+1.36}_{-1.98}, 1.53^{\circ}{}^{+0.93}_{-0.78})$. Within this region, three gamma sources have been reported in 4LAC. Sorted by the nearest angular distance, the gamma-ray sources 4FGL J2226.6+0210, 4FGL J2226.8+0051, and 4FGL J2223.3+0102, with angular separations of 0.65°, 0.67°, and 1.07°. The first and last are associated with blazars, but 4FGL J2226.8+0051, located at RA, Dec = (336.8°, 1.53°) (Charlot et al. 2020) is a gamma-ray source associated with the quasar PKS B2224+006 (Allen et al. 2011; Jackson et al. 2002), with a redshift $z = 2.25$.

The Figure 2 displays the ligth curve in of the 4FGL J2226.8+0051 over 15 years of data acquisition by Fermi-LAT. The Hop method identified flare activity from MJD 59063 to MJD 59243, with a duration of 180 days. From this figure, we can see that at the time of neutrino detection, the light curve does not show signals of activity that are different from the baseline recorded up to the time of neutrino detection. In a time window containing one week after and before the detection done by IceCube, we found that the statistical significance at the neutrino position is 0.0σ in the energy band of 0.1-100 GeV. Meanwhile, the 4FGL J2226.8+0051 source has a statistical significance of 1.17σ. These values impede the claim of the direct confirmation of 4FGL J2226.8+0051 as a neutrino progenitor. In addition, we found that an event with such an angular separation is poorly associated with statistical arguments.

[7] https://ned.ipac.caltech.edu/
[8] http://cdsportal.u-strasbg.fr/
[9] https://fermi.gsfc.nasa.gov/ssc/data/access/lat/10yr_catalog/ap_lcs.php
[10] https://github.com/swagner-astro/lightcurves/blob/main/README.md

Table 1. Spatial correlation found between high energy neutrinos reported by IceCube and γ-ray sources with a FSRQ counterpart reported by Fermi-LAT

IceCube Neutrino	Position (RA$^{\circ}{}^{+\Delta RA}_{-\Delta RA}$, Dec$^{\circ}{}^{+\Delta Dec}_{-\Delta Dec}$)	Energy (TeV)	4FGL Source	Position (RA°, Dec°)	Angular Separation (°)	Counterpart	Redshift
110807A	$(336.80^{+1.36}_{-1.98}, 1.53^{+0.93}_{-0.78})$	108.0	J2226.8+0051	(336.71, 0.86)	0.67	PKS B2224+006	2.25
110930A	$(267.01^{+1.19}_{-1.14}, -4.44^{+0.60}_{-0.79})$	160.0	J1744.2-0353	(266.05, -3.88)	1.10	PKS 1741-03	1.05
120515A	$(198.94^{+1.71}_{-1.41}, 32.00^{+0.97}_{-1.09})$	194.0	J1310.5+3221	(197.63, 32.35)	1.16	OP 313	1.67
-	-	-	J1311.0+3233	(197.75, 32.55)	1.14	RX J131058.8+323335	1.63
120916A	$(182.24^{+1.36}_{-1.71}, 3.88^{+0.67}_{-0.82})$	174.0	J1204.8+0407	(181.20, 4.12)	1.06	MG1 J120448+0408	1.94
130127A	$(352.97^{+1.32}_{-1.01}, -1.98^{+0.97}_{-0.90})$	235.0	J2333.4-0133	(353.36, -1.55)	0.58	PKS B2330-017	1.06
-	-	-	J2335.4-0128	(353.86, -1.47)	1.03	PKS 2332-017	1.18
140114A	$(337.59^{+0.57}_{-0.92}, 0.71^{+0.97}_{-0.86})$	54.0	J2226.8+0051	(336.71, 0.86)	0.89	PKS B2224+006	2.25
141012A	$(63.85^{+2.24}_{-1.36}, 3.21^{+0.90}_{-1.08})$	173.0	J0422.8+0225	(65.70, 2.42)	2.01	PKS 0420+022	2.27
141210A	$(318.12^{+2.33}_{-1.93}, 1.57^{+1.57}_{-1.72})$	154.0	J2118.0+0019	(319.50, 0.32)	1.86	PMN J2118+0013	0.46
150104A	$(272.11^{+1.71}_{-1.54}, 28.76^{+2.41}_{-1.86})$	133.0	J1814.4+2953	(273.61, 29.89)	1.73	B2 1811+29	1.35
150904A	$(133.77^{+0.53}_{-0.88}, 28.08^{+0.51}_{-0.55})$	302.0	J0852.2+2834	(133.06, 28.57)	0.79	B2 0849+28	1.28
150919A	$(279.54^{+1.76}_{-2.29}, 30.35^{+2.19}_{-1.50})$	228.0	J1834.2+3136	(278.56, 31.60)	1.51	4C +31.51	0.59
170308A	$(155.35^{+2.02}_{-1.19}, 5.53^{+0.98}_{-0.90})$	107.0	J1018.4+0528	(154.61, 5.47)	0.73	TXS 1015+057	1.94
181212A	$(316.41^{+1.85}_{-2.02}, -31.0^{+1.68}_{-1.58})$	162.0	J2101.4-2935	(315.36, -29.59)	1.67	PKS 2058-297	1.50
201130A	$(30.54^{+1.10}_{-1.27}, -12.10^{+1.14}_{-1.11})$	203.0	J0206.4-1151	(31.60, -11.85)	1.07	PMN J0206-1150	1.66
211216A	$(316.05^{+2.55}_{-1.93}, 15.79^{+1.62}_{-1.24})$	113.0	J2108.5+1434	(317.14, 14.58)	1.61	OX 110	2.02
220509A	$(334.25^{+1.93}_{-1.41}, 5.38^{+1.65}_{-1.58})$	177.0	J2212.8+0647	(333.21, 6.78)	1.74	TXS 2210+065	1.12
220928A	$(207.42^{+1.41}_{-2.46}, 10.43^{+0.91}_{-0.91})$	143.0	J1342.6+0944	(205.67, 9.73)	1.86	NVSS J134240+094752	0.28
230914A	$(163.83^{+2.55}_{-2.02}, 31.83^{+2.08}_{-1.77})$	168.0	J1102.9+3014	(165.74, 30.24)	2.28	B2 1100+30B	0.38

3.2. IC110930A

On 30 September 2011 at 10:40:59 UTC (MJD 55833.44), IceCube detected the neutrino IC110930A, with an arrival position in RA, Dec = (267.01$^{\circ}{}^{+1.19}_{-1.14}$, -4.44$^{\circ}{}^{+0.60}_{-0.79}$). Within the error region is a gamma-ray source identified in the 4LAC, designated as 4FGL J1744.2-0353, located at R.A. 266.05°and Dec -3.88°. This source exhibited an angular separation of 1.10 ° from the neutrino position. At lower energies, the source 4FGL J1744.2-0353 is linked to FSRQ PKS 1741-03 (Wright et al. 2009), which has a redshift of approximately z = 1.05 (Truebenbach & Darling 2017).

Figure 3 displays the ligth curve of the 4FGL J1744.2-0353. The vertical dashed line represents the neutrino time of arrival at IceCube. The Hop algorithm applied to this light curve shows three flare episodes. The first period was from MJD 55403 to MJD 56543, covering 1140 days; the second was from MJD 58763 to MJD 59243, with a duration of 480 days; and the last was from MJD 59423 to MJD 60100, covering 677 days. We note that the neutrino event occurred on MJD 55834.44 when the first flare was detected. Despite this, we can see from Figure 3 that the light curve does not show a significant increase in the photon rate from this source during this flare period. The statistical significance recorded from this sky region in the gamma-ray band at energies from 0.1-100 GeVGeV, we found that in the spot from the neutrino arrival is 1.28σ. On the other hand, the statistical significance recorded for 4FGL J1744.2-0353 is 0.0σ. With these values, we found that there was no excess emission from an electromagnetic progenitor associated with this event. This is consistent with the probability of serendipity calculated with a low value of 0.07, as shown in Table 2.

It is worth mentioning that IceCube triggered a posterior alert, detecting the neutrino IC220205B, which coincided with this gamma-ray source on February 5, 2022, at 20:08:10.59 UTC. A golden alert with an arrival direction of R.A., Dec = (266.80$\pm$0.51°, -3.58 ± 0.51°) (IceCube Collaboration 2022). Nevertheless, the Fermi-LAT collaboration reported that in this sky region, in the energy band of 0.1-300 GeV, they did not find evidence of an excess of gamma rays that could be considered a possible progenitor for this neutrino (Garrappa et al. 2022).

3.3. IC120515A

On May 15, 2012, at 23:00:59.27 UTC (MJD 56061.95), the IceCube observatory detected the neutrino IC120515A, which had a reconstructed energy of approximately 194 TeV and an arrival direction of R.A., Dec = (198.94$^{+1.71}_{-1.41}$ °, 32.00$^{+0.97}_{-1.09}$ °). Three gamma-ray sources were identified in the 4LAC catalog within the error region of the arrival direction. The sources include 4FGL J1310.5+3221, located at coordinates (RA,Dec) = (197.6324°, 32.35°), with an angular distance of 1.16 ° from the neutrino position. This source is related to FSRQ OP 313 (Ballet et al. 2020) with a redshift of z = 0.997 (Schneider et al. 2010). The second object is 4FGL J1311.0+3233 located at (RA,Dec) = (197.75°,32.55°), with an angular separation of approximately 1.14 ° from the neutrino location. The gamma-ray source is linked to RX J131058.8+323335, identified as an FRSQ with a redshift of z = 1.63 (Alam et al. 2015). The final source is 4FGL J1321.9+3219, a blazar located at (RA,Dec) = (200.48°, Dec 32.33°), exhibiting an angular separation of approximately 1.35°.

Figure 4 displays the light curves detected by Fermi-LAT in the energy range of 0.1-100 GeV for the two FSRQs inside the error region. At the top of the figure, in subpanel 4a, we can see the 4FGL J1310.5+3221 count rate. Meanwhile, 4FGL J1311.0+3233 is displayed in the lower panel 4b. During the periods from 55763 to 55793 with a duration of 30 days, from 56183 to 56303 with

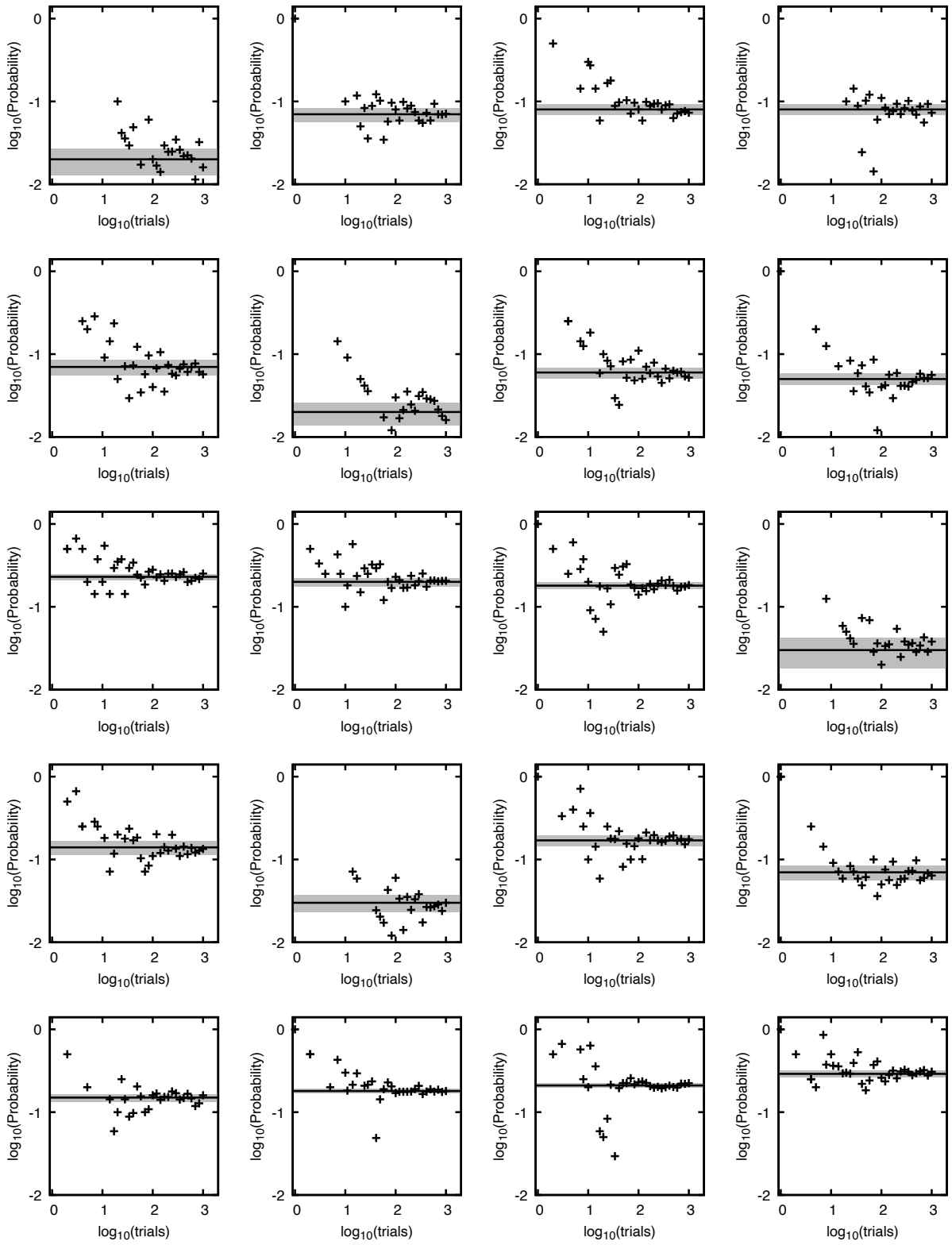

Figure 1. Serendipity probability for each spatial correlation found. As can be seen, the match rate remains low ($\sim 1\%$) for all sources. The black line shows the probability obtained and the gray filled area denotes 1σ of the mean value.

a duration of 120 days, from MJD 56723 to MJD 56963 with a duration of 240 days, from MJD 58613 to MJD 58943 with a duration of 330 days, from MJD 59243 to MJD 59303 with a duration of 60 days, and the last one from MJD 59453 to MJD 60116 with a duration of 663 days. At the time of neutrino detection, the source was not in a flaring period. However, we found that

Table 2. Average value of the Monte Carlo processes done to compute each spatial association found.*

IceCube event	FSRQ Associated	Serendipity probability
IC110807A	PKS B2224+006	0.02 ± 0.007
IC110930A	PKS 1741-03	0.07 ± 0.013
IC120515A	OP 313	0.08 ± 0.012
IC120515A	RX J131058.8+323335	0.08 ± 0.012
IC120916A	MG1 J120448+0408	0.07 ± 0.015
IC130127A	PKS B2330-017	0.02 ± 0.006
IC130127A	PKS 2332-017	0.06 ± 0.009
IC140114A	PKS B2224+006	0.05 ± 0.008
IC141012A	PKS 0420+022	0.23 ± 0.020
IC141210A	PMN J2118+0013	0.20 ± 0.023
IC150104A	B2 1811+29	0.18 ± 0.017
IC150904A	B2 0849+28	0.03 ± 0.012
IC150919A	4C +31.51	0.14 ± 0.027
IC170308A	TXS 1015+057	0.03 ± 0.007
IC181212A	PKS 2058-297	0.17 ± 0.026
IC201130A	PMN J0206-1150	0.07 ± 0.014
IC211216A	OX 110	0.15 ± 0.016
IC220509A	TXS 2210+065	0.18 ± 0.010
IC220928A	NVSS J134240+094752	0.21 ± 0.013
IC230914A	B2 1100+30B	0.29 ± 0.026

*The first column lists the IceCube events. The second column list the FRSQ associated to the gamma-ray source listed in the 4LAC-DR3 and finally, the third column show the average value with their standard deviation of the values obtained in the Monte Carlo Processes.

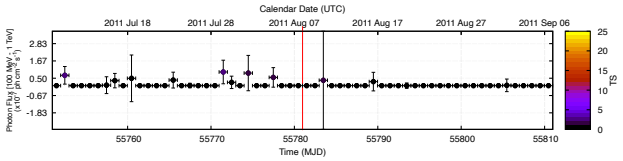

Figure 2. Photon rate detected by Fermi-LAT from 4FGL J2226.8+0051 over 15 years of data acquisition. The vertical dashed line denotes the time of neutrino detection by IceCube. In other hand, the vertical shaded region represents the area in which is detected a flare period accord on Hop criteria.

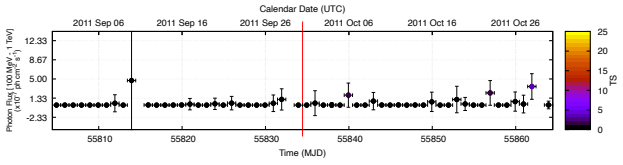

Figure 3. The same as Figure 2 but for 4FGL J1744.2-0353 and the detection of the neutrino IC110930A.

seven days before and after neutrino detection, the statistical significance of 4FGL J1310.5+3221 was 0.0σ. The statistical significance recorded at the neutrino position was 1.13σ, which shows that there is no evidence that 4FGL J1310.5+3221 could be the progenitor of this neutrino. IceCube triggered multiple alerts from the position of this source in April (MJD 58949),

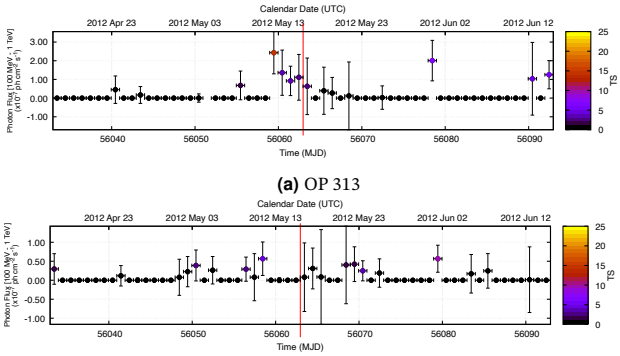

(a) OP 313

(b) RX J131058.8+323335

Figure 4. The same as Figure 2 but for 4FGL J1310.5+3221 at top. At bottom 4FGL J1311.0+3233. From the two cases with the detection of the neutrino IC120515A.

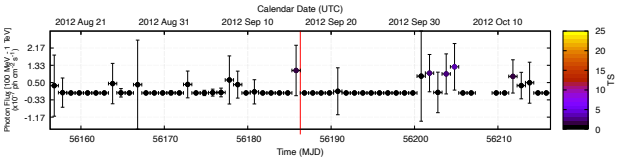

Figure 5. The same as Figure 2 but for 4FGL J1204.8+0407 and the detection of the neutrino IC120916A.

May (MJD 58970, 58986), and August (MJD 59088) in 2020, and February (MJD 60365) and March (MJD 60399) in 2024 (The Fact Collaboration et al. 2022; Briscioli 2023). Despite this, Briscioli (2023) point out that the 2012 alert is the most post-trial relevant event concerning OP 313. We found that a serendipity probability of 0.08 was not statistically significant enough to claim a real association under these considerations.

In contrast, the sub-panel 4b shows a similar behavior for RX J131058.8+323335, where the Hop algorithm finds six flare periods: from MJD 55763 to MJD 55793 with a duration of 30 days, from MJD 56183 to MJD 56303 with a duration of 120 days, from MJD 56723 to MJD 56873 with a duration of 150 days, from MJD 58613 to MJD 58943 with a duration of 330 days, from MJD 59243 to MJD 59303 with a duration of 60 days, and finally from MJD 59453 to MJD 60116 with a duration of 663 days. In the case of 4FGL J1310.5+3221, neutrino detection was outside any flare activity of the electromagnetic counterpart. In a time window centered at the neutrino detection time, one week before and after, we found that the point of the sky where the neutrino was detected had a statistical significance of 0.0σ, while the 4FGL J1311.0+3233 had a statistical significance of 4.85σ which is weak evidence of gamma-ray activity in the energy range of 0.1-100 GeV from this source. Finally, we found that the serendipity probability associated with this event was 0.08, which was also inconclusive.

3.4. IC120916A

On September 16, 2012, at 07:19:38 UTC (MJD 56185.30), IceCube observed the neutrino event IC120916A with an arrival direction of R.A., Dec = $(182.24^{\circ}{}^{+1.36}_{-1.71}, 3.88^{\circ}{}^{+0.67}_{-0.82})$ and an energy of 174 Te. Within the error zone of the reconstructed position, a gamma-ray source identified in the 4LAC, designated 4FGL J1204.8+0407, is situated at (RA,Dec) = (181.20°,4.12°), with an angular separation of 1.06°. This source is related to MG1 J120448+0408, which is classified as an FSRQ with a redshift of z = 1.94.

The Figure 5 displays the light curve from this source, the Hop algorithm does not show any presence of a flare state. In the previous time window centered on neutrino detection, we found that in the neutrino position, the statistical significance was 0.0σ, while in the Fermi-LAT source, the statistical significance was 0.06σ. This scenario is not favorable for considering MG1 J120448+0408 as a neutrino progenitor if we consider the serendipity probability of 0.07.

3.5. IC130127A

On January 27, 2013, at 06:43:11 UTC (MJD 56318.27), the IceCube Observatory detected the neutrino IC130127A. The reconstructed arrival position is (RA,Dec) = ($337.59^{\circ}{}^{+0.57}_{-0.92}$, $0.71^{\circ}{}^{+0.97}_{-0.86}$), with an energy of 235 TeV. Within the error region of the reconstructed neutrino position, two sources were identified in the 4LAC. The first object, 4FGL J2333.4-0133, is situated at R.A. 353.36 °, Dec -1.55° with an angular separation of approximately 0.58°. The second object, 4FGL J2335.4-0128, is located at (RA,Dec) = (353.86°,-1.47°), exhibiting an angular separation of 1.03°. Both are linked to a flat-spectrum radio quasar (FSRQ). The initial object is linked to PKS B2330-017, a quasar at a distance of z= 1.05. The other FSRQ is PKS 2332-017 (Véron-Cetty & Véron 2010), located at a distance of z = 1.19 (Lyke et al. 2020).

The Figure 6 displays the rate light curve from these sources. In the top sub-panel 6a we can appreciate the case of PKS B2330-017 in the gamma-ray band of 0.1-100 GeV. The Hop algorithm identified three flare states: from MJD 55223 to MJD 57173 with a duration of 1950 days, from MJD 58313 to MJD 58853 with a duration of 540 days, and from MJD 59423 to MJD 60055 with a duration of 632 days. Neutrino time detection occurs in the first period. In a time window from one week before to one week after the detection, we found that the LAT source had a statistical significance of 0.71σ. Meanwhile, the position of the best-fit reconstruction had a 0.0σ. Moreover, the serendipity probability that we found is 0.02, which is also a weak argument to determine whether this source is a neutrino progenitor.

In the other hand, the sub panel 6b shows the rate light curve of PKS 2332-017 in the energy band of 0.1-100 GeV. Using the Hop algorithm, we found four flare periods: from MJD 55253 to MJD 56003 with a duration of 750 days, from MJD 56333 to MJD 56873 with a duration of 540 days, from MJD 58673 to MJD 58733 with a duration of 60 days, and finally from MJD 59544 to MJD 60085 with a duration of 541 days. Neutrino detection occurs near the start of the second period. In this case, the statistical significance of the Fermi-LAT source is 1.11σ in the time interval of one week before and after the neutrino detection, while the neutrino arrival point has a statistical significance of 0.0σ.

3.6. IC140114A

The IceCube Observatory recorded the neutrino event IC140114A on January 14, 2014, at 21:04:09 UTC (MJD 56669.87). The optimal fit reconstructed for this neutrino was (RA,Dec) = ($337.59^{\circ}{}^{+0.57}_{-0.92}$, $0.71^{\circ}{}^{+0.97}_{-0.86}$) with an energy of 54 TeV. Within the error region of this neutrino, two gamma-ray sources were identified by LAT and documented in the 4LAC. The first object is 4FGL J2227.9+0036, located at (RA,Dec) = (336.98°, Dec 0.61°), associated with PMN J2227+0037, a blazar (Véron-Cetty & Véron 2010), exhibiting an angular distance of 0.61 ° from the neutrino position. The second object is 4FGL J2226.8+0051, located at an angular distance of 0.89 ° from the neutrino position. This source was also a candidate for the IC110807A neutrino.

Figure 7 displays the rate of the light curve from this source. The Hop algorithm showed a flare period from MJD 59063 to MJD 59243 with a duration of 180 days. The time detection from neutrinos by IceCube is far from this period. Searching in a time window from one week before and after, centered on the time of neutrino detection, we found that the point of arrival direction of the neutrino had a statistical significance of 0.0σ. Meanwhile, 4FGL J2226.8+0051 has a statistical significance of 1.62σ. Considering this and the low probability of serendipity of 0.05, we found that this source has weak criteria for being associated with this neutrino.

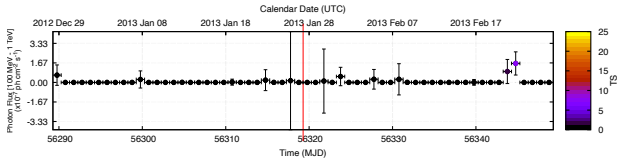

(a) PKS B2330-017

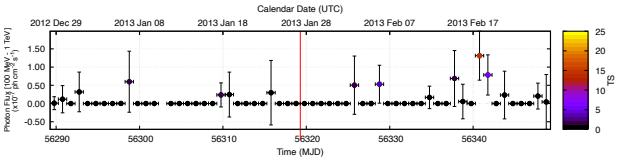

(b) PKS 2332-017

Figure 6. The same as Figure 2 but for 4FGL J2333.4-0133 at top. At bottom 4FGL J2335.4-0128. From the two cases with the detection of the neutrino IC130127A.

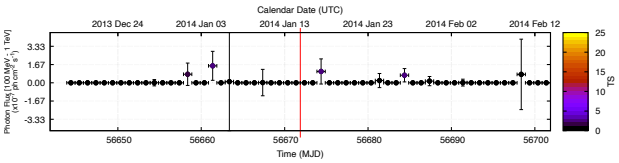

Figure 7. The same as Figure 2 but for 4FGL J2226.8+0051 and the detection of the neutrino IC140114A.

3.7. IC141012A

On October 12, 2014, at 18:01:14 UTC (MJD 56940.75), the neutrino IC141012A was detected by the IceCube observatory. Its energy was 173 TeV, and its arrival direction was (RA,Dec) = ($63.85\ ^{\circ}{}^{+2.24}_{-1.36}$, $3.21\ ^{\circ}{}^{+0.90}_{-1.08}$). There are two known gamma-ray sources in the 4LAC within the error region of this neutrino. The Blazar candidate PKS 0409+025 (Germani et al. 2021) is linked to 4FGL J0412.3+0239, which is located at (RA,Dec) = (63.09°, 2.65°), with an angular separation of 0.94°. The second is the 4FGL J0422.8+0225 in (RA,Dec) = (65.70°, 2.42°), which has a greater angular separation of 2.01°. This source is related to the farthest source in our sample, PKS 0420+022, a quasar (Abdo et al. 2010) located at z = 2.27 (Truebenbach & Darling 2017).

Figure 8 shows the rate light curve of PKS 0420+022 detected by Fermi-LAT. We note that the Hop algorithm did not identify any possible flare periods. In the time window centered on the neutrino position, one week before and after, we found that the neutrino position had a statistical significance of 0.0σ, the same as the 4FLG point source. This event had a 0.05 chance of being associated with it. The event was not associated with them.

3.8. IC141210A

With an energy of 154 TeV and an arrival position of (RA,Dec) = ($318.12\ ^{\circ}{}_{+2.33-1.93}$, $1.57\ ^{\circ}{}^{+1.57}_{-1.72}$), IceCube detected the neutrino IC141210A on December 10, 2014, at 20:20:47 UTC

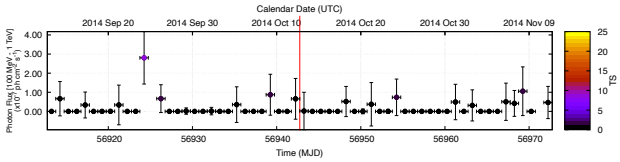

Figure 8. The same as Figure 2 but for 4FGL J0422.8+0225 and the detection of the neutrino IC141012A.

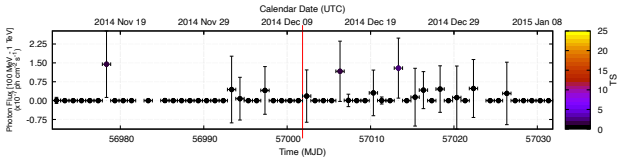

Figure 9. The same as Figure 2 but for 4FGL J2118.0+0019 and the detection of the neutrino IC141210A.

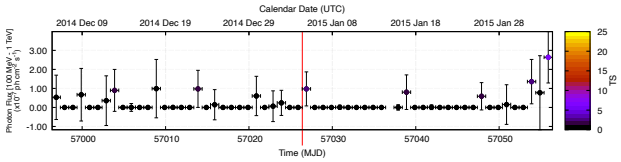

Figure 10. The same as Figure 2 but for 4FGL J1814.4+2953 and the detection of the neutrino IC150104A.

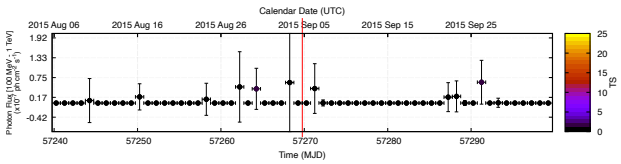

Figure 11. The same as Figure 2 but for 4FGL J0852.2+2834 and the detection of the neutrino IC150904A.

(MJD 57000.84). The 4FGL J2118.0+0019, a 4LAC source, is located inside the error region of the arrival position at (RA, Dec) = (319.50°, 0.32°), with an angular separation of 1.86 ° from the neutrino position. This item is located at z = 0.46 (Albareti et al. 2017) and is associated with an FRSQ at lower energies with PMN J2118+0013 (Healey et al. 2007).

Figure 9 displays the count rate light curve from 4FGL J2118.0+0019 in the energy range of 0.1-100 GeV. As can be seen in it, the Hop algorithm suggests a flare period from MJD 54713 to MJD 55043 with a duration of 330 days. Neutrino detection is far from this suggested period. In addition, the statistical significance, computed in a time window of one week before and after the neutrino detection at the neutrino position, is 0.0σ, while the statistical significance of 4FGL J2118.0+0019 in the same time window is 0.14σ. The probability of serendipity from this source was 0.20.

3.9. IC150104A

On January 4, 2015, at 09:34:31 UTC (57025.39), IceCube detected the neutrino IC150104A, which possessed an energy of 133 TeV and an arrival position of (RA,Dec) = (272.11 $^{\circ}{}^{+1.71}_{-1.54}$, 28.76 $^{\circ}{}^{+2.41}_{-1.86}$). Within the error region of the arrival position, there exist three 4LAC sources, specifically 4FGL J1803.5+2756, 4FGL J1809.7+2910, and 4FGL J1814.4+2953. The analysis began with 4FGL J1809.7+2910, which is placed at R.A., Dec = 272.44°, 29.17°, holding an angular separation of 0.50 ° from the neutrino position. This source is classified as a BL Lac at lower energies with MG2 J180948+2910 (Massaro et al. 2009). In contrast, 4FGL J1814.4+2953 is a gamma-ray source located at (RA,Dec) = (273.61°, 29.89°), which produces an angular separation of 1.73°. This source is associated with an FSRQ at lower energies to B2 1811+29 (Sowards-Emmerd et al. 2005), with a distance of z = 1.36 (Sowards-Emmerd et al. 2005). Finally, the 4FGL J1803.5+2756 located at (RA,Dec) = (270.87°,27.94°) with an angular separation from the neutrino of approximately 1.36°, associated with BL LAC, NVSS J180341+275404 (D'Abrusco et al. 2019).

Figure 10 shows the rate light curve from the gamma-ray source 4FGL J1814.4+2953 in the energy range of 0.1-100 GeV. The Hop algorithm exhibited a flare period on the light curve from MJD 57442 to MJD 57505, lasting 63 d; however, the neutrino arrival time differed by 440 d. In the gamma-ray band, we found that 4FGL J1814.4+2953 has a statistical significance of 0.0σ. The neutrino arrival point has a statistical significance of 1.3σ. Furthermore, the serendipity probability for this source was 0.18. However, these arguments are not strong enough to claim an association between the two phenomena.

3.10. IC150904A

With an energy of 228 TeV and an arrival position of (RA,Dec) = (133.77 $^{\circ}{}^{+0.53}_{-0.88}$, 28.08 $^{\circ}{}^{+0.51}_{-0.55}$), IceCube detected the neutrino IC150904A on September 4, 2015, at 18:13:54 UTC (MJD 57268.75). A 4LAC source, the 4FGL J0852.2+2834, located at (RA,Dec) = (133.06°, 28.57°), with an angular separation of 0.79 ° from the neutrino position, is located inside the arrival position error region. A counterpart to 4FGL J0852.2+2834 at lower energies is located at z = 1.28 (Alam et al. 2015), with the FRSQ B2 0849+28 (Allen et al. 2011). Another source lies in the position error region, the 4FGL J0854.0+2753 placed at R.A., Dec = 133.51°, 27.88°, which is associated with lower energies to the source SDSS J085410.16+275421.7, which is classified as a BL Lac (Plotkin et al. 2008).

We can appreciate the rate light curve in Figure 11 in the range of 0.1-100 GeV. We note that the Hop algorithm does not show any flare period on the gamma-ray light curve from 4FGL J0852.2+2834. In addition, the week before and after the neutrino detection time, we found that 4FGL J0852.2+2834 has a statistical significance of 0.0σ. Meanwhile, the neutrino position had a statistical significance of 1.48σ. This event had a serendipity probability of 0.03. This evidence is insufficient to support the hypothesis that these sources are related.

3.11. IC150919A

IceCube identified the neutrino IC150919A on 19 September 2015 at 04:56:09 UTC (MJD 57283.20), with an arrival position at R.A., Dec = (267.01 $^{\circ}{}^{+1.19}_{-1.14}$, -4.44 $^{\circ}{}^{+0.60}_{-0.79}$). Within the error region, four gamma-ray sources were identified in the 4LAC. There are: 4FGL J1836.4+3137, 4FGL J1841.3+2909, 4FGL J1834.2+3136, 4FGL J1841.8+3218. We found that J1836.4+3137, J1841.3+2909, and J1841.8+3218 were associated with BL Lac blazars. J1836.4+3137 is associated with RX J1836.2+3136 (D'Abrusco et al. 2013), with an angle separation of approximately 1.32 ° from the neutrino position. J1841.3+2909 is associated with MG3 J184126+2910 (Healey et al. 2007), with a distance of 1.39 ° from the best-fit neutrino position. In addition, J1841.8+3218, which is associated with RX J1841.7+3218, is a BL Lac blazar (D'Abrusco et al. 2014) with an angular separation of 2.10°. Finally, 4FGL J1834.2+3136, located at coordinates (RA,Dec) = (278.56°,31.60°). This source

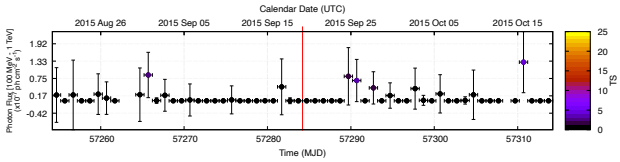

Figure 12. The same as Figure 2 but for 4FGL J1834.2+3136 and the detection of the neutrino IC150919A.

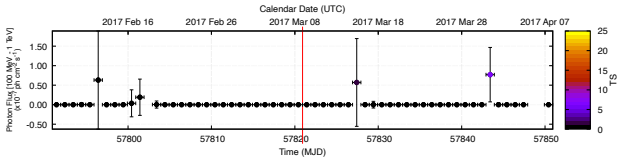

Figure 13. The same as Figure 2 but for 4FGL J1018.4+0528 and the detection of the neutrino IC170308A.

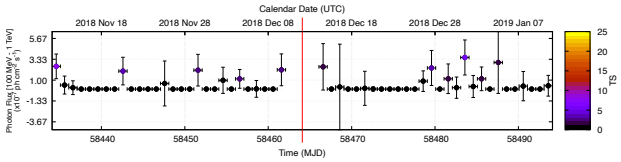

Figure 14. The same as Figure 2 but for 4FGL J2101.4-2935 and the detection of the neutrino IC181212A.

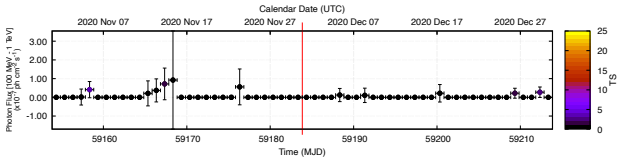

Figure 15. The same as Figure 2 but for 4FGL J0206.4-1151 and the detection of the neutrino IC201130A.

exhibited an angular separation of 1.51 ° from the neutrino position. At lower energies, the source 4FGL J1834.2+3136 is linked to FSRQ 4C +31.51 (Becker et al. 1991), which has a redshift of z = 0.59 (Guo et al. 2022).

Fig. 12 displays the rate light curve from 4FGL J1834.2+3136. The Hop algorithm did not suggest any flare activity. Additionally, within the one-week window preceding and following the neutrino observation, we find that the neutrino arrival position and the 4FGL J1834.2+3136 have a statistical significance of 0.0σ.

3.12. IC170308A

On March 8, 2017 at 22:11:49 UTC (MJD 57820.92), IceCube detected the neutrino IC170308A, located at (RA, Dec) = ($155.35^{\circ}{}^{+2.02}_{-1.19}$, $5.53^{\circ}{}^{+0.98}_{-0.90}$). Three gamma-ray sources were identified within the error region in the 4LAC. The identified sources are: 4FGL J1019.7+0511, 4FGL J1026.9+0608, and 4FGL J1018.4+0528. J1019.7+0511 and J1026.9+0608 were identified as sources associated with the blazar category. 4FGL J1019.7+0511 is associated with NVSS J101948+051327, a candidate blazar (Ballet et al. 2023) with an angular separation of 0.53 ° from the neutrino position. In the case of 4FGL J1026.9+0608, a gamma-ray source associated with NVSS J102703+060934, a BL Lac (Mao et al. 2016) with an angular separation of 1.51 ° from the neutrino position. Finally, the gamma-ray source 4FGL J1018.4+0528 is associated with an FRSQ in the low-energy band with TXS 1015+057 (Sowards-Emmerd et al. 2005). This source is located at R.A., Dec = 154.61°, 5.47°, separated by approximately 0.73°from the best-fit neutrino position. The distance from this source is approximately z = 1.94 (Alam et al. 2015).

Figure 13 displays the rate light curve from 4FGL J1018.4+0528 in the energy range of 0.1-100 GeV, where the Hop algorithm does not give clues of flaring activity. Additionally, within one week between and after neutrino detection, the statistical significance of 4FGL J1018.4+0528 was 0.0σ. The best-fit position from this neutrino has a statistical significance of 0.85σ. The serendipity probability of this association was extremely weak, reaching a value of 0.03.

3.13. IC181212A

On December 12, 2018, at 02:02:43 UTC (MJD 58464.08), IceCube detected the neutrino IC181212A, which possessed an energy of 162 TeV and was located at R.A., Dec = (316.41 $^{\circ}{}^{+1.85}_{-2.02}$, -31.0 $^{\circ}{}^{+1.68}_{-1.58}$). The 4LAC source, 4FGL J2101.4-2935, is located at (RA,Dec) = (315.36 °, -29.59°), with an angular separation of 1.67°, from the neutrino position, and is encompassed within the arrival position error region. This object is located at z = 1.50 (Truebenbach & Darling 2017) and is identified as an FRSQ at lower energies in association with PKS 2058-297 (Véron-Cetty & Véron 2010).

We analyze the rate light curve in Figure 14 in the energy range of 0.1-100 GeV. The Hop method indicates that there are no flare periods in the gamma-ray light curve of 4FGL J2101.4-2935. In the one-week period preceding and before neutrino detection, 4FGL J2101.4-2935 exhibited a statistical significance of 0.0σ, but the position of the neutrino demonstrated a statistical significance of 2.82σ. This occurrence has a serendipity probability of 0.03. These data undermine the premise that these sources are correlated.

3.14. IC201130A

On November 30, 2020, at 20:21:46 UTC (MJD 59183.84), IceCube identified the neutrino IC201130A, which had an energy of 203 TeV and was positioned at (RA,Dec) = ,($30.54^{\circ}{}^{+1.10}_{-1.27}$, $-12.10^{\circ}{}^{+1.14}_{-1.11}$). The 4LAC source, 4FGL J0206.4-1151, is located at R.A. 31.60°, Dec -11.85°, with an angular separation of 1.07°, from the neutrino position, and lies inside the arrival position error zone. This object is located at z = 1.66 (Ackermann et al. 2018) and is classified as an FRSQ at lower energies in connection with PMN J0206-1150 (Healey et al. 2007).

We can examine the rate light curve in Figure 15 within the range of 0.1-100 GeV. The Hop approach suggests three flare phases in the gamma-ray light curve of J0206.4- 1151: from MJD 54983 to MJD 55133 with a duration of 150 days, from MJD 55373 to MJD 55733 with a duration of 360 days, and finally from MJD 57473 to MJD 58523 with a duration of 1050 days. However, the neutrino detection time was outside these flare episodes. During the week prior to and following the neutrino detection, J0206.4-1151 showed a statistical significance of 0.0σ, whereas the neutrino location indicated a statistical significance of 1.28σ. The likelihood of this occurrence was 0.07.

3.15. IC211216A

On December 16, 2021, at 07:07:38 UTC (MJD 59564.29), IceCube detected the neutrino IC211216A, which exhibited an energy of 113 TeV and was located at R.A., Dec = (316.05 $^{\circ}{}^{+2.55}_{-1.93}$, 15.79 $^{\circ}{}^{+1.62}_{-1.24}$). The 4LAC source, 4FGL J2108.5+1434, is situated at R.A. 317.14°and Dec 14.58°. It has an angular separation of 1.61 ° from the neutrino position and is located within the arrival position error zone. The object was located at z = 2.02 (Gattano et al. 2018)

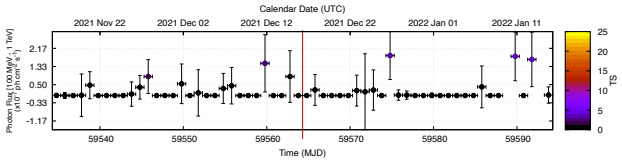

Figure 16. The same as Figure 2 but for 4FGL J2108.5+1434 and the detection of the neutrino IC211216A.

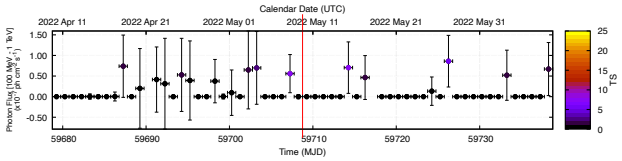

Figure 17. The same as Figure 2 but for 4FGL J2212.8+0647 and the detection of the neutrino IC220509A.

and is categorized as an FRSQ at lower energies in relation to OX 110 (Healey et al. 2007).

The light curve of the rate shown in Figure 16 can be analyzed in the range of 0.1-100 GeV. The Hop approach indicates the presence of a moderate flare phase in the gamma-ray light curve of 4FGL J2108.5+1434, from MJD 55595 to MJD 56033, with a duration of 438 days, but the neutrino detection was far from this activity. In the week preceding and following neutrino detection, 4FGL J2108.5+1434 exhibited a statistical significance of 0.96σ, whereas the location of the neutrino indicated a statistical significance of 0.18σ. The probability of this event was 0.15. These data contradict the claim that multiple sources are correlated.

3.16. IC220509A

On 9 May 2022 at 18:19:04 UTC (MJD 59709.76), IceCube identified the neutrino IC220509A, positioned at R.A., Dec = $334.25^{\circ}{}^{+1.93}_{-1.41}$, $5.38^{\circ}{}^{+1.65}_{-1.58}$). Three gamma-ray sources were detected within the error zone of the neutrino. The recognized sources are: 4FGL J2215.4+0544, 4FGL J2212.8+0647, and 4FGL J2224.5+0353. J2224.5+0353 and J2215.4+0544 were classified as blazars. 4FGL J2224.5+0353 is linked to 1RXS J222426.5+035445, a candidate Blazar (Haakonsen & Rutledge 2009), exhibiting an angular separation of 2.39 ° from the neutrino location. For 4FGL J2215.4+0544, a gamma-ray source linked to NVSS J221513+054454, a BL Lac (Dong et al. 2018), there exists an angular separation of 0.53 ° from the neutrino position. The gamma-ray source 4FGL J2212.8+0647 is linked to an FRSQ in the low-energy band with TXS 2210+065 (Healey et al. 2007). This source is situated at R.A., Dec = 333.21°, 9.73°, separating 1.89 ° from the optimal neutrino position. The distance from this source is z = 1.12 (Peña-Herazo et al. 2021).

Figure 17 illustrates the light curve of 4FGL J2212.8+0647 in the energy range of 0.1-100 GeV, indicating that the Hop algorithm suggests a discrete increase of activity, from MJD 56873 to 57803 with a duration of 930 days. Furthermore, throughout the one-week interval surrounding the neutrino detection, the statistical significance of 4FGL J2212.8+0647 was 3.64σ, whereas the position of the best-fit from this neutrino exhibited a statistical significance of 0.0σ. The likelihood of serendipity associated with this correlation was relatively low, at 0.18.

3.17. IC220928A

The IceCube Neutrino Observatory detected the neutrino IC220928A on September 28, 2022, at 12:32:38 UTC (MJD 59851.52), with an energy of 143 TeV and an arrival direction of (RA,Dec) = ($207.42^{\circ}{}^{+1.41}_{-2.46}$, $10.43^{\circ}{}^{+0.91}_{-0.91}$). Within the error region of this neutrino, two gamma-ray sources were reported in the 4LAC. The object 4FGL J1351.3+1115 positioned at (RA,Dec) = (207.84°,11.25°), is linked to the BL LAC: RX J1351.3+1115 (Plotkin et al. 2008), exhibiting an angular separation of 0.92°. The second object, exhibiting a larger angular separation of 1.86°, was identified as 4FGL J1342.6+0944, positioned at R.A., Dec = 205.67°, 9.73°. This source is linked to NVSS J134240+094752, an FSRQ (Yao et al. 2019) with a redshift of z = 0.28.

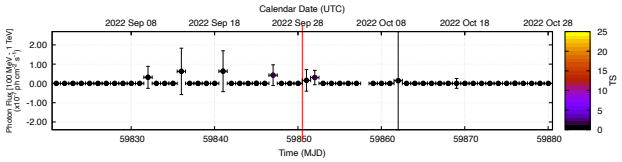

Figure 18. The same as Figure 2 but for 4FGL J1342.6+0944 and the detection of the neutrino IC220928A.

Figure 18 illustrates the light curve rate of NVSS J134240+094752 as detected by Fermi-LAT. The Hop algorithm did not identify any potential flaring periods. Additionally, our analysis revealed that within the time window centered on the neutrino position, specifically one week before and after, the statistical significance of the neutrino position was 0.98σ. In addition, the 4FLG point source had a statistical significance of 0.47σ. The probability of this event being associated was 0.05; therefore, it did not appear to be associated with them.

3.18. IC230914A

The event IC230914A was detected on 14 September 2023 at 05:21:03 UTC (MJD 60202.22), with an arrival direction of RA, Dec = ($163.83^{\circ}{}^{+2.55}_{-2.02}$, $31.83^{\circ}{}^{+2.08}_{-1.77}$). One gamma-ray source has been reported in this region in the 4LAC. The gamma-ray sources are 4FGL J1102.9+3014, with an angular separation of 2.28°. These sources are linked to the FSRQ. 4FGL J1102.9+3014, positioned at(RA,Dec) = 165.74°and Dec=30.24°, is a gamma-ray source associated with B2 1100+30B (Sowards-Emmerd et al. 2005), exhibiting a redshift of z = 0.38 (Ahn et al. 2012).

Figure 19 presents the light curve of 4FGL J1102.9+3014. The Hop method does not identify flare activity from this source. The figure indicates that at the time of neutrino detection, the light curve did not exhibit any activity signals beyond the baseline recorded before detection. Within one week of detection by IceCube, the statistical significance at the neutrino position was found to be 1.20σ in the energy range of 0.1-100 GeV. Additionally, the 4FGL J1102.9+3014 source exhibits statistical significance of 1.49σ. These values prevent the direct confirmation of 4FGL J1102.9+3014 as a neutrino progenitor. The probability of an event with this angular separation was found to be weak, reaching a value of 0.29, which does not provide a strong argument to believe that these two objects are correlated with statistical arguments.

4. Model

In a pure leptonic scenario, the non-thermal emission of the SED of AGNs is described by a relativistic population of electrons, in which the first peak of the spectra is described by synchrotron radiation of electrons. The second peak is attributed to Synchrotron Self-Compton radiation resulting from

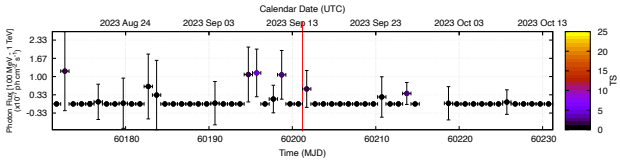

Figure 19. The same as Figure 2 but for 4FGL J1102.9+3014 and the detection of the neutrino IC230914A.

the interactions between electrons and synchrotron photons. In this scenario, we cannot expect neutrino emission; thus, a hadronic component is injected. We assume that a relativistic population of protons is co-accelerated within the electron population. In this paradigm, protons can interact with low-energy photons and produce a hadronic flux of γ-rays with a neutrino flux, which is a product of neutral and charged pion decay, respectively (Fraija et al. 2020).

We suggest that the extended Spectral Energy Distribution of the FRSQ, which we propose as a neutrino progenitor, can be characterized as a one-zone emission region that includes a lepto-hadronic contribution. Therefore, a relativistic population of electrons and protons is injected into the emission region, where the protons interact with low-energy photons via photo-pion ($p\gamma$) interactions. We assume a standard spherical blob of radius R'_b moving with a Lorentz factor $\Gamma = (1-\beta^2)^{-1/2}$, where β is the velocity normalized to the speed of light. Thus, the comoving volume of the blob is $V'_b = \frac{4}{3}\pi R'^3_b$. This implies that the emitting volume is restricted by the light travel time given by $t'_{\rm var} \gtrsim R'_b/c$, since blazars are astrophysical objects that show a high variability that can range from time-scales of the order of seconds to years. An angle θ exists between the velocity of the jet of the FSRQ and the observer line of sight expressed as $\theta = \arccos(\mu)$, and the Doppler factor is defined as $\delta_D = [\Gamma(1-\beta\mu)]^{-1}$.

The model assumes that the electrons cool due to synchrotron radiation and synchrontron self-Compton (SSC), which could account for the extended spectral energy distribution. The protons cool down via photo-hadronic processes, producing a non-thermal hadronic γ-ray contribution with a signature of high-energy neutrinos. Protons require a low-energy radiation field to produce pγ interactions, suggesting that this radiation originates from the broad-line region.

Inside the blob, both electrons and protons are accelerated up to the ultra-relativistic regime, which must produce the observed radiation. Electrons are assumed to have a homogeneous and isotropic distribution given by a broken power-law function (e.g. see Fraija et al. 2017b, 2020)

$$N'_e(\gamma'_e) = K'_e \begin{cases} \gamma'^{-\alpha_{e,1}}_e, & \gamma'_{e,\rm min} \le \gamma'_e \le \gamma'_{e,\rm br} \\ \gamma'^{\alpha_{e,2}-\alpha_{e,1}}_{e,\rm br}\gamma'^{-\alpha_{e,2}}_e, & \gamma'_{e,\rm br} \le \gamma'_e \le \gamma'_{e,\rm max}\,, \end{cases} \quad (1)$$

where $\gamma'_{\rm e,min}, \gamma'_{\rm e,br}, \gamma'_{\rm e,max}$ are the minimum, break, and maximum Lorentz factors of ultrarelativistic electrons, respectively, and K'_e is the normalization constant. On the other hand, we assume protons are distributed homogeneously and isotropically during the equilibrium stage, given by

$$N'_p(\varepsilon'_p) = K'_p \left(\frac{\varepsilon'_p}{m_p c^2}\right)^{-\alpha_p} \qquad \varepsilon'_{p,\rm min} \le \varepsilon'_p \le \varepsilon'_{p,\rm max}\,, \quad (2)$$

where K'_p is the normalization constant, α_p is the proton spectral index, and $\varepsilon'_{p,\rm min}$ and $\varepsilon'_{p,\rm max}$ correspond to the minimum and maximum energies in the comoving frame, respectively.

4.1. Synchrotron Radiation

In the presence of a magnetic field (B), relativistically charged particles move along the field lines while losing energy via synchrotron radiation. The power radiated by an electron distribution is (Blumenthal & Gould 1970; Finke et al. 2008; Saugé & Henri 2004; Aguilar-Ruiz et al. 2023c)

$$J'_{\rm s}(\varepsilon'_s) = \frac{\sqrt{3}e^3 B'}{2\pi\hbar m_e c^2}\int_{\gamma'_{e,\rm min}}^{\gamma'_{e,\rm max}} d\gamma'_e N'_e(\gamma'_e)\, R_{\rm syn}(x)\,, \quad (3)$$

where $\hbar$ is the reduced Planck constant e is the electron charge, $x = \varepsilon'_s/\varepsilon'_{\rm ch}$, the characteristic energy is given by $\varepsilon'_{\rm ch} = \frac{3eB'\hbar}{2m_e c}\gamma'^2_e \sin\theta$ and $\sin\theta$ is the pitch angle, the function $R_{\rm syn}$ is given by Finke et al. (2008).

4.2. Inverse-Compton Scattering

When an electron moves within a radiation field, it generates Compton scattering, and the energy lost by the synchrotron electrons in each collision results in the production of high-energy photons. The total emissivity coefficient produced by an isotropic electron population is (Blumenthal & Gould 1970)

$$J'_{ic}(\varepsilon'_c) = \frac{3}{4}c\sigma_{\rm T}\varepsilon'_c \int_{\frac{\varepsilon'_c}{m_e c^2}} d\gamma'_e \frac{N'_e(\gamma''_e)}{\gamma'^2_e}\int d\varepsilon' \frac{n'_{\rm ph}(\varepsilon')}{\varepsilon'} F_c(q,\Gamma_e)\,. \quad (4)$$

Finally, the inverse Compton radiation was calculated using the above equation, but with different photon spectra for SSC and EIC emissions. The total seed photon distribution is

$$n'_{\rm ph}(\varepsilon') \simeq \frac{J'_s(\varepsilon')}{4\pi R'^2 c\,\varepsilon'} + \delta_D\,(n_{\rm BLR}(\varepsilon') + n_{\rm DT}(\varepsilon')) \quad (5)$$

4.3. Photopion Process

The photopion process results in the production of nonstable secondary products, that is, π^0 and $\pi^\pm$ mesons (Kelner & Aharonian 2008):

$$p + \gamma \to n_0\pi^0 + n_+\pi^+ + n_-\pi^- + ... \quad (6)$$

where n_0, n_-, n_+ are the multiplicities of neutral, negative, and positive charged pions, respectively. Pions decay into final stable particles as

$$\pi^0 \to \gamma\gamma \quad (7)$$
$$\pi^+ \to e^+ + \nu_e + \bar{\nu}_\mu + \nu_\mu \quad (8)$$
$$\pi^- \to e^- + \bar{\nu}_e + \nu_\mu + \bar{\nu}_\mu\,. \quad (9)$$

The proton energy threshold to photopion production is given by the condition to produce a single rest mass pion; by considering the seed's photons in the blob frame we obtain

$$\varepsilon'^{p\pi}_{p,\rm th} = \frac{m_\pi^2 + 2m_\pi m_p}{4\varepsilon'} \approx 70\,{\rm PeV}\left(\frac{\varepsilon'}{\rm eV}\right)^{-1}. \quad (10)$$

The production rate of stable particles is given by Kelner & Aharonian (2008)

$$Q'^{p\pi}_i(\varepsilon'_i) = \int \frac{d\varepsilon'_p}{\varepsilon'_p} N'_p(\varepsilon'_p) \int d\varepsilon'\, n'_{\rm ph}(\varepsilon')\, \Phi_i(\eta, x), \qquad (11)$$

where the label i represents the particles $\gamma, \nu, \bar{\nu}, e^-, e^+$, the function Φ_i is parametrized by the authors, and they define the parameters $\eta = \frac{4\varepsilon'_p\varepsilon'}{m_p^2c^4} > 0.303$ and $x = \frac{\varepsilon'_i}{\varepsilon'_p}$.

Finally, the luminosity of the jet can be obtained as the contribution of the electron, proton, and magnetic field luminosities (Celotti & Ghisellini 2008; Aguilar-Ruiz et al. 2023a,b);

$$L_j = \sum_{i=e,p,B} L_i, \qquad (12)$$

where $L_i \simeq \pi r_d^2 \Gamma^2 U_i$ where, r_d is the emission region size defined as $r_d = \delta_D \tau_{\rm v,min}/(1+z)$ with $t_{\rm var,min}$ as the minimum time of variability. As we are dealing with blazars, we assume that $\delta_D \approx \Gamma$. So, $U_e = m_e N_e \langle\gamma_e\rangle$ $, = m_e \int_{\gamma_{\rm min}}^{\gamma_{\rm max}} \frac{dn_e}{d\gamma_e} d\gamma_e$, $U_p = N_p m_p$ and $U_B = B'^2/(8\pi)$ are the electron, proton and magnetic field densities, respectively.

4.4. Modeling the Spectral Energy Distributions

The fitting method chosen is the Monte Carlo Markov Chain (MCMC) technique implemented in the `emcee` package (Foreman-Mackey et al. 2013) for Python. To obtain a suitable set of priori parameters for each source listed in Table 1 a previous fit was performed using the `LMFIT` (Newville et al. 2014) python package. Once the prior parameters were obtained, an MCMC sampler was built using 512 walkers with 12,000 steps. The parameters involved in the MCMC process were the parameters for the leptonic model, such as the magnetic field (B), Doppler factor (δ_D), minimum, break, and maximum Lorentz factors from the electron population ($\gamma'_{\rm min}$, $\gamma'_{\rm break}$ and $\gamma'_{\rm max}$ respectively) with the shape of a broken power law population with slope p and normalization constant K'_e. For the hadronic component, the power law index of the proton distribution was fixed to 2, and the target photons taken into account came from the Narrow and Broad emission lines on the seed photon distribution, allowing the constant normalization to be free K_p.

5. Results and Conclusion

Our study analyzed data spanning 12 years from IceCube, along with 14 years of gamma-ray emissions detected by Fermi-LAT, as documented in 4FGL-DR4 (Abdollahi et al. 2020; Ballet et al. 2020). We focused on γ-ray sources with angular separations of less than two degrees (2°) from the best-fit neutrino positions. This analysis revealed 20 spatial coincidences between the FSRQ γ-ray sources listed in 4LAC-DR3 and the neutrinos observed by IceCube. Additionally, motivated by the neutrino flare associated with the IceCube-170922A event, which was observed from TXS 0506+056 (IceCube Collaboration et al. 2018b,a), we examined the γ-ray observations for each quasar within a time frame of one week (± one week) following the trigger event.

Figures 20 and 21 show the SED of each object found with spatial coincidence with a neutrino. The SED was constructed using historical data. The values of the best-fit parameters are listed in Table 3. Each row in these figures corresponds to the SED of the sources listed in Table 1. For each SED archival data obtained from NED[11] and from the CDS portal[12] (Abdollahi et al. 2020), were fitted assuming a leptohadronic model to describe the SED. Figure 20 shows the results of the photo-pion decay products, considering the $p\gamma$ interactions with a low photon field from the Narrow Line Region (NLR) and Fig. 21 from the Broad Line Region (BLR). The dotted gray line in both figures indicates this contribution. The leptonic component is shown as long-dashed lines. The first peak ($\sim 10^{12-14}$ Hz) is due to the synchrotron of the relativistic electrons, while the second peak ($\sim 10^{22-24}$ Hz) is described by a lepton component produced by Inverse Compton scattering together with a hadronic component of photons ($\sim 10^{25-26}$ Hz) that decay from neutral pions created by interactions of protons with seed photons from the NLR and the BRL, respectively. In the case of the high-energy component, the flux was attenuated by the extragalactic background light (EBL) by a factor $\exp(-\tau(\mathrm{E,z}))$ with the factor τ provided by Franceschini et al. (2008), and parameterized by polynomial functions in this study.

The values listed in Tables 3 and 4 as a consequence of the MCMC method are in the range of those reported in the literature (e.g. see Finke et al. 2008; Aguilar-Ruiz et al. 2022, 2021). For example, the Doppler factor lies in $20 \leq \delta_D \leq 100$ and the volume of the emission region lies in values of $\sim 10^{17}$ cm^3 which corresponds to a minimum variability time of $\sim$ 1days (Abdo et al. 2011a,b; Fraija et al. 2017a, 2019), which is lower than that recorded in observation campaigns from other sources (Kataoka et al. 2001; Abdo et al. 2011a; Dunlop et al. 2003). Compared to the predicted Eddington luminosity $L_{\rm Edd} \sim 10^{48}$ erg s^{-1}, based on the evaluation of the supermassive black hole mass $M_{\rm BH} \sim 10^9\, M_\odot$ (Wagner 2008; McLure & Dunlop 2004), the calculated proton luminosity (L_p) is proportional to a small amount. By analyzing the magnetic field, electron and proton densities, and their respective ratios $U_{\rm i}/U_{\rm j}$ derived and listed in Table 4, we can observe that the potential existence of the principle of equipartition can be inferred from the results.

In addition, we adopted an electron/proton population described by a power law. This is a consequence of considering that the acceleration of particles lies in a First-Order Fermi acceleration, in which the acceleration and scape particles are in a steady state (Kardashev 1962). However, when the diffusive term is not negligible, the solution becomes a log-parabola shape, which corresponds to a Second-Order Fermi acceleration regime. This scenario was explored by Massaro et al. (2006); Dermer et al. (2015), in which the blazar Mkn 501 spectra were studied. They found that the broadband SED was successfully described by assuming this paradigm, in which the gamma-ray band had an internal absorption rather than the EBL.

Recently, Anjum et al. (2020) studied a sample of the LAT Bright AGN Sample and compared it with the values obtained in this work. Across the sample, the magnetic energy densities (u_B) are typically well below the combined particle energy densities ($u_e + u_p$), indicating particle-dominated jets, which is in agreement with previous blazar studies. The electron spectral indices ($p \sim 2.0 - 3.3$) and Lorentz break factors ($\gamma_{br} \sim 10^{3-4.5}$) are consistent with the expectations of shock-acceleration processes and subsequent radiative cooling. Sources with the highest inferred γ_{br} and γ_{max} tend to display comparatively higher electron luminosities (L_e). Moreover, according to the theory of spectral curvature discussed by Anjum et al. (2020), stronger cooling or weaker stochastic acceleration leads to an increased curvature of

[11] https://ned.ipac.caltech.edu/
[12] http://cdsportal.u-strasbg.fr/

Table 3. Best-fit values for the leptonic components in the SED of each source associated to a 4FGL in the arrival region of the neutrino detected by IceCube

Name	$\log(B/\mathrm{G})$	δ_D	$\log(K_e)$	p	$\log(\gamma_{\rm min})$	$\log(\gamma_{\rm br})$	$\log(\gamma_{\rm max})$	$\log(t_{\rm var}/\mathrm{s})$	$\log(K_p^{\rm BLR})$	$\log(K_p^{\rm NLR})$
PKS B2224+006	1.46	1.56	49.00	3.34	2.78	3.33	5.68	5.93	30.89	17.52
PKS 1741-03	1.50	1.52	45.20	3.22	2.41	4.28	5.05	5.47	28.72	19.67
OP 313	1.04	1.60	49.91	2.18	2.15	2.82	5.00	5.52	20.35	11.30
RX J131058.8+323335	1.81	1.65	45.29	2.85	2.06	3.96	4.28	4.55	25.72	16.68
MG1 J120448+0408	1.77	1.32	46.54	2.55	2.15	3.68	5.04	5.04	25.35	16.30
PKS B2330-017	0.62	1.48	47.66	2.00	2.12	3.96	4.85	5.92	20.41	11.36
PKS 2332017	2.03	1.68	47.06	2.47	1.91	3.15	5.01	4.25	22.98	13.94
PKS B2224+006	—	—	—-	—	—	—	—	—	—	—
PKS 0420022	1.26	1.49	47.32	2.51	1.91	3.23	5.23	4.62	26.16	17.12
PMN J2118+0013	0.88	1.52	45.29	2.75	2.68	4.58	5.11	5.55	24.02	14.98
B2 1811+29	1.81	1.91	44.33	2.32	1.22	3.70	5.07	3.52	21.20	12.15
B2 0849+28	1.03	2.18	43.35	2.41	1.62	4.20	5.00	3.41	20.86	11.81
4C +31.51	1.01	1.69	45.24	2.38	1.62	4.19	5.00	4.75	21.27	12.23
TXS 1015+057	0.66	1.63	48.57	2.50	2.48	3.60	5.01	5.36	23.79	14.75
PKS 2058-297	1.66	1.52	47.74	2.73	2.13	3.59	5.22	5.73	25.34	16.29
PMN J0206-1150	1.51	1.66	46.90	2.72	2.31	3.79	5.13	5.25	25.68	16.63
OX 110	1.07	1.48	46.74	2.39	1.99	3.67	5.03	4.86	22.73	13.69
TXS 2210+065	0.87	1.45	47.68	2.23	2.27	3.60	5.05	5.13	22.23	13.19
NVSS J134240+094752	1.61	1.74	45.86	2.56	2.84	3.70	5.29	4.42	23.46	14.42
B2 1100+30B	1.72	1.35	43.41	2.67	2.17	4.60	5.00	4.50	25.81	16.76

Note: All log values are in base 10.

Table 4. Derived quantities.

Name	u_B ($\times10^{-4}$)	u_e ($\times10^{-4}$)	u_p ($\times10^{-4}$)	$U_B/(U_e+U_p)$	L_B ($\times10^{45}$)	L_e ($\times10^{45}$)	L_p ($\times10^{45}$)	L_j ($\times10^{45}$)
PKS B2224+006	0.34	0.01	12.98	0.03	0.36	0.01	13.75	14.13
PKS 1741-03	0.40	0.12	2.96	1.30×10^{-1}	0.09	0.03	0.66	0.78
OP 313	0.05	0.06	3.42×10^{4}	1.41×10^{-6}	0.03	0.04	2.10×10^{4}	2.10×10^{4}
RX J131058.8+323335	1.68	9.74	84.12	0.02	0.01	0.06	0.55	0.62
MG1 J120448+0408	1.42	218.31	1.46×10^{5}	9.72×10^{-6}	5.50×10^{-4}	0.08	56.60	56.70
PKS B2330-017	0.01	0.01	6.10×10^{6}	1.17×10^{-9}	0.01	0.01	7.64×10^{6}	7.64×10^{6}
PKS 2332017	4.57	8.34	5.28×10^{3}	8.64×10^{-4}	0.01	0.03	17.20	17.20
—	—	—	—-	—	—	—	—	—
PKS 0420022	6.31	2.18	6.59×10^{5}	9.56×10^{-6}	0.08	0.03	8.22×10^{3}	8.22×10^{3}
PMN J2118+0013	0.02	0.09	26.09	8.98×10^{-4}	1.45×10^{-3}	5.40×10^{-3}	1.61	1.61
B2 1811+29	1.73	22.05	5.75×10^{3}	2.99×10^{-4}	0.01	0.18	45.90	46.00
B2 0849+28	0.05	0.05	223.15	2.08×10^{-4}	0.27	0.29	1.32×10^{3}	1.32×10^{3}
4C +31.51	0.04	0.93	1.32×10^{3}	3.21×10^{-5}	2.76×10^{-3}	0.06	86.00	86.00
TXS 1015+057	0.01	0.91	1.61×10^{4}	5.27×10^{-7}	1.49×10^{-3}	0.16	2.83×10^{3}	2.83×10^{3}
PKS 2058-297	0.84	0.17	8.95×10^{3}	9.33×10^{-5}	0.17	0.03	1.79×10^{3}	1.79×10^{3}
PMN J0206-1150	0.42	0.25	157.71	2.69×10^{-3}	0.05	0.03	17.60	17.70
OX 110	0.05	2.46	4.23×10^{5}	1.30×10^{-7}	5.71×10^{-3}	0.26	4.40×10^{4}	4.40×10^{4}
TXS 2210+065	0.02	0.04	8.57×10^{5}	2.63×10^{-8}	0.02	0.04	$7.69\mathrm{e}\times10^{5}$	7.69×10^{5}
NVSS J134240+094752	0.68	2.80	0.35	0.22	2.35×10^{-4}	9.65×10^{-4}	1.21×10^{-4}	1.32×10^{-3}
B2 1100+30B	1.14	0.65	46.33	0.02	8.67×10^{-3}	4.92×10^{-3}	0.35	0.37

the SED. In our sample, this is broadly supported by the trend of a lower γ_{br} and a steeper p for objects with larger u_p and lower L_e. These inter-comparisons reinforce the physical consistency of our fits and provide additional justification for our modeling selection.

It is also observed that in the IR-optical bands, an excess is present that is not quite fitted by synchrotron emission; this effect can also be appreciated in the gamma-ray band, where the SSC does not fit as well; this can be explained by the SED being built with historical data and discrepancies with the expected behavior predicted by models due to the higher variability exhibited in these objects. For example, Ghisellini et al. (2017), who revisited the blazar sequence detected by Fermi-LAT over four years of operations, found that a significant proportion of FSRQs exhibited indications of thermal emission from the accretion disk, which influenced the optical-UV spectrum. This point has also been discussed by Ghisellini (2016). When they normalized the entire SED to the peak of the disk emission, a reduced scatter in the other bands is found, especially in the radio and in the X-rays (in the γ-rays the variability amplitude is so large to hide the reduction of the scatter) and thus can be taken as model independent evidence that the disk and the jet luminosity are related. This highlights

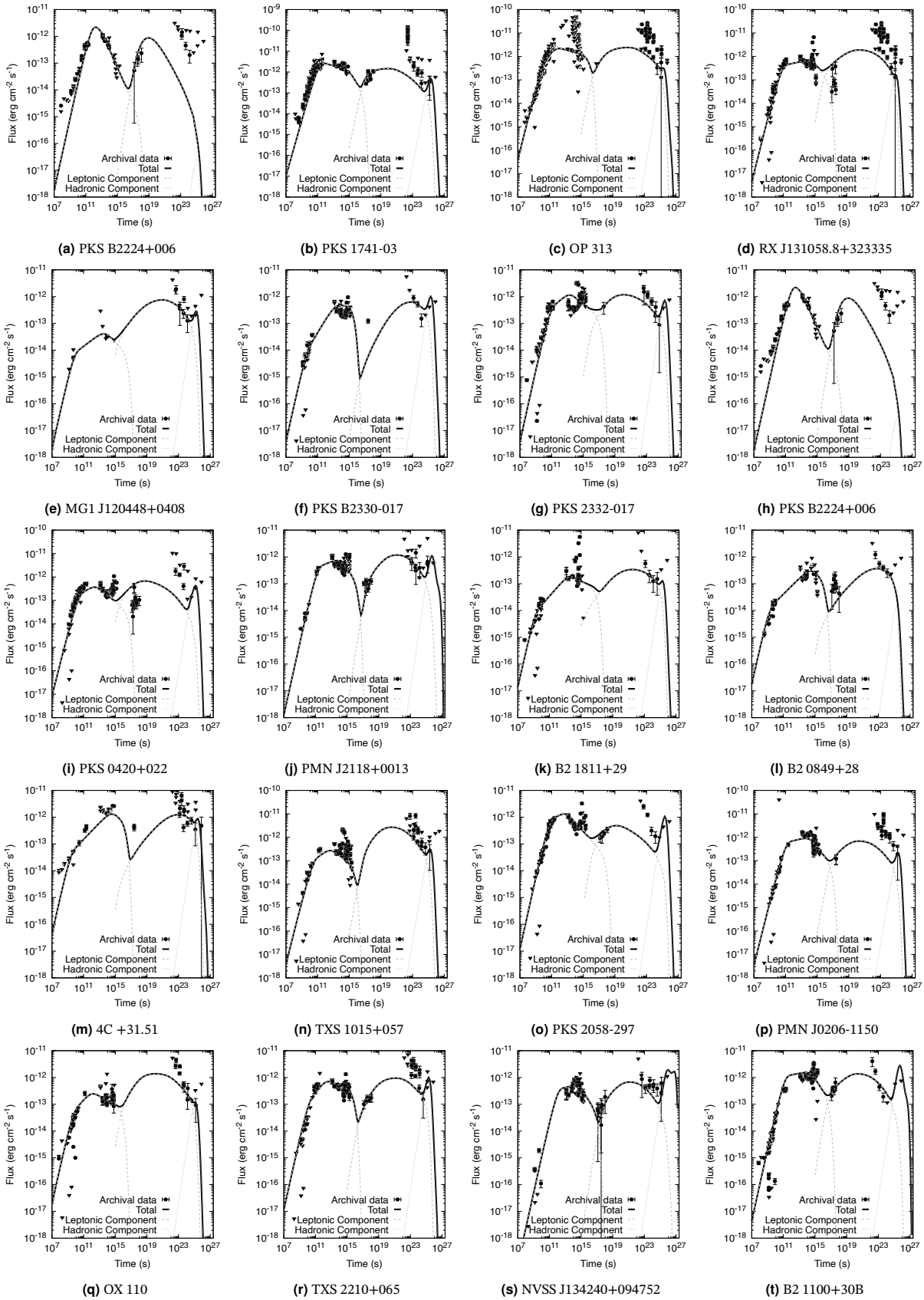

(a) PKS B2224+006 **(b)** PKS 1741-03 **(c)** OP 313 **(d)** RX J131058.8+323335

(e) MG1 J120448+0408 **(f)** PKS B2330-017 **(g)** PKS 2332-017 **(h)** PKS B2224+006

(i) PKS 0420+022 **(j)** PMN J2118+0013 **(k)** B2 1811+29 **(l)** B2 0849+28

(m) 4C +31.51 **(n)** TXS 1015+057 **(o)** PKS 2058-297 **(p)** PMN J0206-1150

(q) OX 110 **(r)** TXS 2210+065 **(s)** NVSS J134240+094752 **(t)** B2 1100+30B

Figure 20. Spectral Energy Distribution of the γ-ray sources detected by Fermi-LAT associated with Quasars within the sky region enclosed within the High Energy neutrino arrival direction. In this particular case, we have assumed that the target photons to produce hadronic reactions comes from the narrow line region.

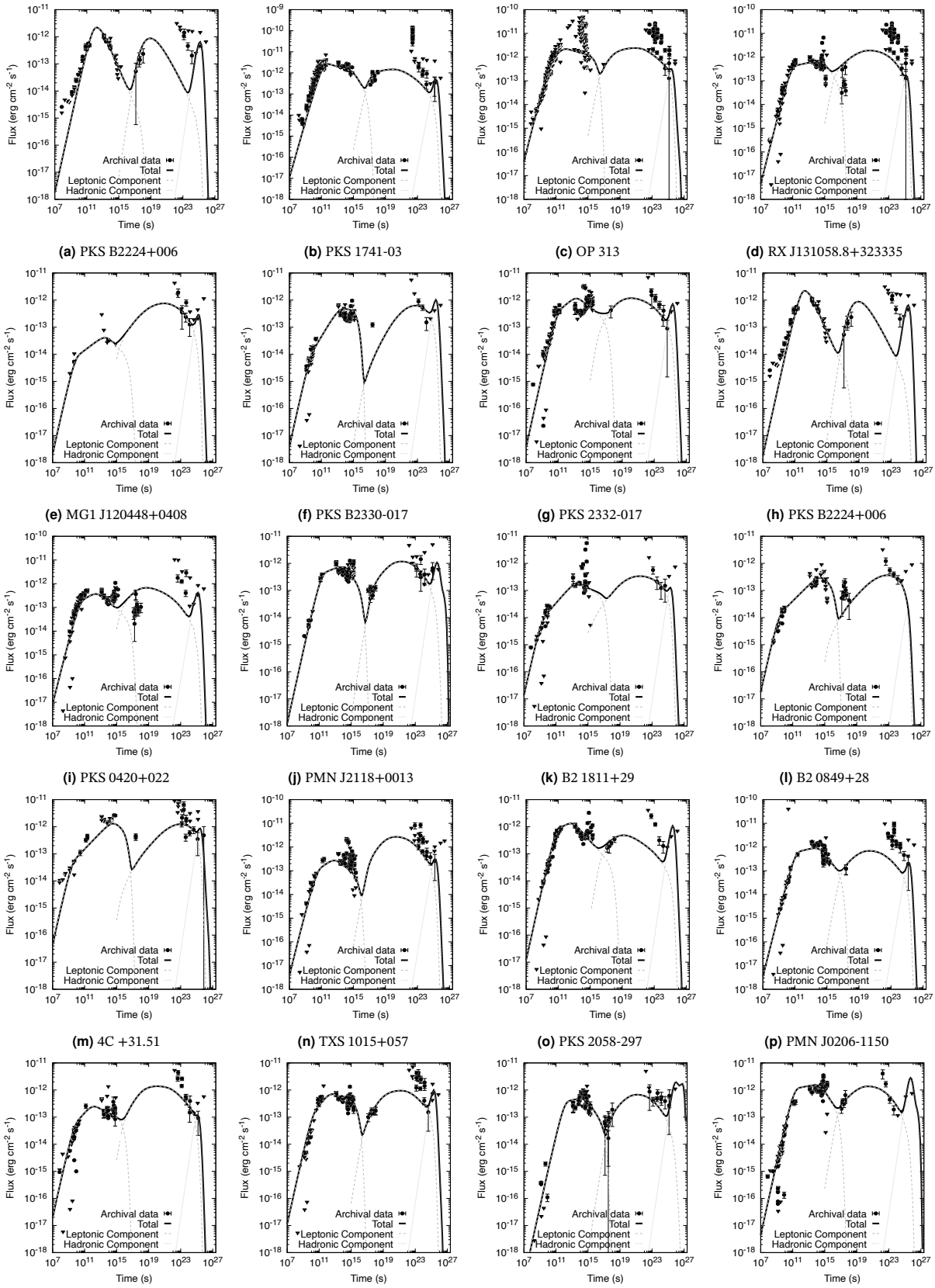

(a) PKS B2224+006 **(b)** PKS 1741-03 **(c)** OP 313 **(d)** RX J131058.8+323335

(e) MG1 J120448+0408 **(f)** PKS B2330-017 **(g)** PKS 2332-017 **(h)** PKS B2224+006

(i) PKS 0420+022 **(j)** PMN J2118+0013 **(k)** B2 1811+29 **(l)** B2 0849+28

(m) 4C +31.51 **(n)** TXS 1015+057 **(o)** PKS 2058-297 **(p)** PMN J0206-1150

(q) OX 110 **(r)** TXS 2210+065 **(s)** NVSS J134240+094752 **(t)** B2 1100+30B

Figure 21. Same as table 20 but considering the target photons of the $p\gamma$ interaction comes from the broadline region.

the importance of multi-wavelength observational campaigns on this type of object, since blazars are highly variable on multiple timescales, and the use of heterogeneous epochs can misrepresent the true emission state and lead to biased parameter inference in, for example, single-zone SSC or EC models. Accordingly, while our synchrotron peak is constrained and modeled, we refrain from attempting an overly strict fit of the high-energy component when using non-simultaneous data.

A comparison of our fitted parameters with the calculated jet energy indicates a consistent physical model in which relativistic collisions and stochastic processes collaboratively influence the observed emissions of FSRQs. The predominance of particle energy densities over magnetic fields supports efficient acceleration and radiative cooling in particle-dominated jets. Although limited by the non-simultaneous nature of the data, the overall agreement between our findings and previous investigations of blazars at multiple wavelengths corroborates the robustness of our modeling method. This highlights the need for synchronized observations that integrate future multi-frequency observation campaigns in AGNs. These data will be crucial for constraining time-dependent models and understanding the relationship between high-energy neutrino generation and jet energy in blazars.

6. Facilities

We acknowledge the use of public data and analysis tools provided by the Fermi Science Support Center (FSSC) and Fermi-LAT Collaboration, as well as data from the IceCube Neutrino Observatory available through the IceCube Public Data Portal. This research used the NASA/IPAC Extragalactic Database (NED), operated by the Jet Propulsion Laboratory, California Institute of Technology, under contract with NASA, and data products from the Sloan Digital Sky Survey (SDSS). We also thank the Infrared Processing and Analysis Center (IPAC) for providing access to the archival resources that supported this work.

This work was supported by the Postdoctoral Program of the Instituto de Física, UNAM. NF acknowledges financial support from UNAM-DGAPA-PAPIIT through grant IN112525. HLV and AG acknowledge financial support from UNAM-DGAPA-PAPIIT through grant IN102223 and SECIHTI grant CF-2023-I-645. JD acknowledges financial support from UNAM-DGAPA-PAPIIT through the grant IN116325. We also thank the referee for his/her helpful comments on how to improve this work.

REFERENCES

Abbasi, R., Ackermann, M., Adams, J., et al. 2023, ApJS, 269, 25, doi: 10.3847/1538-4365/acfa95

Abdo, A. A., Ackermann, M., Ajello, M., et al. 2010, ApJ, 715, 429, doi: 10.1088/0004-637X/715/1/429

—. 2011a, ApJ, 727, 129, doi: 10.1088/0004-637X/727/2/129

—. 2011b, ApJ, 736, 131, doi: 10.1088/0004-637X/736/2/131

Abdollahi, S., Acero, F., Ackermann, M., et al. 2020, ApJS, 247, 33, doi: 10.3847/1538-4365/ab6bcb

Abdollahi, S., Acero, F., Baldini, L., et al. 2022, ApJS, 260, 53, doi: 10.3847/1538-4365/ac6751

Ackermann, M., Ajello, M., Baldini, L., et al. 2018, ApJS, 237, 32, doi: 10.3847/1538-4365/aacdf7

Aguilar-Ruiz, E., Fraija, N., & Galván-Gámez, A. 2023a, JHEAp, 38, 1, doi: 10.1016/j.jheap.2023.02.001

—. 2023b, EPJC, 83, 338, doi: 10.1140/epjc/s10052-023-11523-w

Aguilar-Ruiz, E., Fraija, N., Galván-Gámez, A., & Benítez, E. 2022, MNRAS, 512, 1557, doi: 10.1093/mnras/stac591

Aguilar-Ruiz, E., Fraija, N., Joshi, J. C., Galvan-Gamez, A., & de Diego, J. A. 2021, PhRvD, 104, 083013, doi: 10.1103/PhysRevD.104.083013

Aguilar-Ruiz, E., Galván-Gámez, A., & Fraija, N. 2023c, Galaxies, 11, 117, doi: 10.3390/galaxies11060117

Ahn, C. P., Alexandroff, R., Allende Prieto, C., et al. 2012, ApJS, 203, 21, doi: 10.1088/0067-0049/203/2/21

Ajello, M., Angioni, R., Axelsson, M., et al. 2020, ApJ, 892, 105, doi: 10.3847/1538-4357/ab791e

Ajello, M., Baldini, L., Ballet, J., et al. 2022, ApJS, 263, 24, doi: 10.3847/1538-4365/ac9523

Alam, S., Albareti, F. D., Allende Prieto, C., et al. 2015, ApJS, 219, 12, doi: 10.1088/0067-0049/219/1/12

Albareti, F. D., Allende Prieto, C., Almeida, A., et al. 2017, ApJS, 233, 25, doi: 10.3847/1538-4365/aa8992

Allen, J. T., Hewett, P. C., Maddox, N., et al. 2011, MNRAS, 410, 860, doi: 10.1111/j.1365-2966.2010.17489.x

Anjum, M. S., Chen, L., & Gu, M. 2020, ApJ, 898, 48, doi: 10.3847/1538-4357/ab99a1

Atwood, W. B., Abdo, A. A., Ackermann, M., et al. 2009, ApJ, 697, 1071, doi: 10.1088/0004-637X/697/2/1071

Ballet, J., Bruel, P., Burnett, T. H., Lott, B., & The Fermi-LAT collaboration. 2023, arXiv:2307.12546, doi: 10.48550/arXiv.2307.12546

Ballet, J., Burnett, T. H., Digel, S. W., & Lott, B. 2020, arXiv:2005.11208, doi: 10.48550/arXiv.2005.11208

Becker, R. H., White, R. L., & Edwards, A. L. 1991, ApJS, 75, 1, doi: 10.1086/191529

Blumenthal, G. R., & Gould, R. J. 1970, RvMP, 42, 237, doi: 10.1103/RevModPhys.42.237

Bose, D., & Rakshit, S. 2021, High Energy Astrophysical Neutrinos (Springer. OCLC), doi: 10.1007/978-3-030-91258-1

Briscioli, A. 2023, Lauree magistrali, Dipartimento di Fisica e Astronomia "Galileo Galilei" - DFA, https://hdl.handle.net/20.500.12608/65401

Celotti, A., & Ghisellini, G. 2008, MNRAS, 385, 283, doi: 10.1111/j.1365-2966.2007.12758.x

Charlot, P., Jacobs, C. S., Gordon, D., et al. 2020, A&A, 644, A159, doi: 10.1051/0004-6361/202038368

Cowan, G., Cranmer, K., Gross, E., & Vitells, O. 2011, EPJC, 71, 1554, doi: 10.1140/epjc/s10052-011-1554-0

D'Abrusco, R., Álvarez Crespo, N., Massaro, F., et al. 2019, ApJS, 242, 4, doi: 10.3847/1538-4365/ab16f4

D'Abrusco, R., Massaro, F., Paggi, A., et al. 2013, ApJS, 206, 12, doi: 10.1088/0067-0049/206/2/12

—. 2014, ApJS, 215, 14, doi: 10.1088/0067-0049/215/1/14

Dermer, C. D., Yan, D., Zhang, L., Finke, J. D., & Lott, B. 2015, ApJ, 809, 174, doi: 10.1088/0004-637X/809/2/174

Dichiara, S., Troja, E., O'Connor, B., et al. 2020, MNRAS, 492, 5011, doi: 10.1093/mnras/staa124

Dong, X. Y., Wu, X.-B., Ai, Y. L., et al. 2018, AJ, 155, 189, doi: 10.3847/1538-3881/aab5ae

Dunlop, J. S., McLure, R. J., Kukula, M. J., et al. 2003, MNRAS, 340, 1095, doi: 10.1046/j.1365-8711.2003.06333.x

Fermi Science Support Development Team. 2019, Fermitools: Fermi Science Tools, Astrophysics Source Code Library, record ascl:1905.011. http://ascl.net/1905.011

Finke, J. D., Dermer, C. D., & Böttcher, M. 2008, ApJ, 686, 181, doi: 10.1086/590900
Foreman-Mackey, D., Hogg, D. W., Lang, D., et al. 2013, PASP, 125, 306, doi: 10.1086/670067
Fraija, N., Aguilar-Ruiz, E., & Galván-Gámez, A. 2020, MNRAS, 497, 5318, doi: 10.1093/mnras/staa2284
Fraija, N., Aguilar-Ruiz, E., Galván-Gámez, A., Marinelli, A., & de Diego, J. A. 2018, MNRAS, 481, 4461, doi: 10.1093/mnras/sty2561
Fraija, N., Benítez, E., Hiriart, D., et al. 2017a, ApJS, 232, 7, doi: 10.3847/1538-4365/aa82cc
—. 2019, ApJS, 245, 18, doi: 10.3847/1538-4365/ab3f28
Fraija, N., Marinelli, A., Galván-Gámez, A., et al. 2017b, APh, 89, 14, doi: 10.1016/j.astropartphys.2017.01.001
Franceschini, A., & Rodighiero, G. 2017, A&A, 603, A34, doi: 10.1051/0004-6361/201629684
Franceschini, A., Rodighiero, G., & Vaccari, M. 2008, A&A, 487, 837, doi: 10.1051/0004-6361:200809691
Gaisser, T. K., Stanev, T., & Tilav, S. 2013, FrPhy, 8, 748, doi: 10.1007/s11467-013-0319-7
Garrappa, S., Buson, S., Franckowiak, A., et al. 2019, ApJ, 880, 103, doi: 10.3847/1538-4357/ab2ada
Garrappa, S., Buson, S., Sinapius, J., et al. 2022, GCN, 31558, 1
Gattano, C., Lambert, S. B., & Le Bail, K. 2018, A&A, 618, A80, doi: 10.1051/0004-6361/201833430
Germani, S., Tosti, G., Lubrano, P., et al. 2021, MNRAS, 505, 5853, doi: 10.1093/mnras/stab1748
Ghisellini, G. 2016, Galaxies, 4, 36, doi: 10.3390/galaxies4040036
Ghisellini, G., Righi, C., Costamante, L., & Tavecchio, F. 2017, MNRAS, 469, 255, doi: 10.1093/mnras/stx806
Gilmore, R. C., Somerville, R. S., Primack, J. R., et al. 2012, MNRAS, 422, 3189, doi: 10.1111/j.1365-2966.2012.20841.x
Guo, H., Barth, A. J., & Wang, S. 2022, ApJ, 940, 20, doi: 10.3847/1538-4357/ac96ec
Haakonsen, C. B., & Rutledge, R. E. 2009, ApJS, 184, 138, doi: 10.1088/0067-0049/184/1/138
Halzen, F., & Hooper, D. 2002, RPPh, 65, 1025, doi: 10.1088/0034-4885/65/7/201
Healey, S. E., Romani, R. W., Taylor, G. B., et al. 2007, ApJS, 171, 61, doi: 10.1086/513742
IceCube Collaboration. 2013, Sci, 342, 1242856, doi: 10.1126/science.1242856
—. 2022, GCN, 31554, 1
IceCube Collaboration, Aartsen, M. G., Ackermann, M., et al. 2018a, Sci, 361, eaat1378, doi: 10.1126/science.aat1378
—. 2018b, Sci, 361, 147, doi: 10.1126/science.aat2890
IceCube Collaboration, Abbasi, R., Ackermann, M., et al. 2022, Sci, 378, 538, doi: 10.1126/science.abg3395
Jackson, C. A., Wall, J. V., Shaver, P. A., et al. 2002, A&A, 386, 97, doi: 10.1051/0004-6361:20020119
Kardashev, N. S. 1962, SvA, 6, 317
Kataoka, J., Takahashi, T., Wagner, S. J., et al. 2001, ApJ, 560, 659, doi: 10.1086/322442
Kelner, S. R., & Aharonian, F. A. 2008, PhRvD, 78, 034013, doi: 10.1103/PhysRevD.78.034013
Lott, B., Gasparrini, D., & Ciprini, S. 2020, arXiv:2010.08406, doi: 10.48550/arXiv.2010.08406
Lyke, B. W., Higley, A. N., McLane, J. N., et al. 2020, ApJS, 250, 8, doi: 10.3847/1538-4365/aba623
Mao, P., Urry, C. M., Massaro, F., et al. 2016, ApJS, 224, 26, doi: 10.3847/0067-0049/224/2/26
Massaro, E., Giommi, P., Leto, C., et al. 2009, A&A, 495, 691, doi: 10.1051/0004-6361:200810161
Massaro, E., Tramacere, A., Perri, M., Giommi, P., & Tosti, G. 2006, A&A, 448, 861, doi: 10.1051/0004-6361:20053644
McLure, R. J., & Dunlop, J. S. 2004, MNRAS, 352, 1390, doi: 10.1111/j.1365-2966.2004.08034.x
Meyer, M., Scargle, J. D., & Blandford, R. D. 2019, ApJ, 877, 39, doi: 10.3847/1538-4357/ab1651
Newville, M., Stensitzki, T., Allen, D. B., et al. 2014, LMFIT: Non-Linear Least-Square Minimization and Curve-Fitting for Python, 0.8.0, Zenodo, doi: 10.5281/zenodo.11813
Peña-Herazo, H. A., Massaro, F., Gu, M., et al. 2021, AJ, 161, 196, doi: 10.3847/1538-3881/abe41d
Petropoulou, M., Oikonomou, F., Mastichiadis, A., et al. 2020, ApJ, 899, 113, doi: 10.3847/1538-4357/aba8a0
Plotkin, R. M., Anderson, S. F., Hall, P. B., et al. 2008, AJ, 135, 2453, doi: 10.1088/0004-6256/135/6/2453
Sahakyan, N., Giommi, P., Padovani, P., et al. 2023, MNRAS, 519, 1396, doi: 10.1093/mnras/stac3607
Saugé, L., & Henri, G. 2004, ApJ, 616, 136, doi: 10.1086/424905
Schneider, D. P., Richards, G. T., Hall, P. B., et al. 2010, AJ, 139, 2360, doi: 10.1088/0004-6256/139/6/2360
Sowards-Emmerd, D., Romani, R. W., Michelson, P. F., et al. 2005, ApJ, 626, 95, doi: 10.1086/429902
The Fact Collaboration, The H. E. S. S. Collaboration, The Icecube Collaboration, et al. 2022, in 37th International Cosmic Ray Conference, 960, doi: 10.22323/1.395.0960
Truebenbach, A. E., & Darling, J. 2017, ApJS, 233, 3, doi: 10.3847/1538-4365/aa9026
Véron-Cetty, M. P., & Véron, P. 2010, A&A, 518, A10, doi: 10.1051/0004-6361/201014188
Wagner, R. M. 2008, MNRAS, 385, 119, doi: 10.1111/j.1365-2966.2008.12850.x
Wagner, S. M., Burd, P., Dorner, D., et al. 2022, in 37th International Cosmic Ray Conference, 868, doi: 10.22323/1.395.0868
Wright, E. L., Chen, X., Odegard, N., et al. 2009, ApJS, 180, 283, doi: 10.1088/0067-0049/180/2/283
Yao, S., Wu, X.-B., Ai, Y. L., et al. 2019, ApJS, 240, 6, doi: 10.3847/1538-4365/aaef88